ANKARA YILDIRIM BEYAZIT UNIVERSITY

GRADUATE SCHOOL OF NATURAL AND APPLIED SCIENCES

INVESTIGATION OF ADHESIVELY-BONDED JOINTS FOR AEROSPACE AND AUTOMOTIVE INDUSTRIES

M.Sc. Thesis by

Mehmet Emin ERCAN

Department of Defense Technologies

May, 2022

ANKARA

INVESTIGATION OF ADHESIVELY-BONDED JOINTS FOR AEROSPACE AND AUTOMOTIVE INDUSTRIES

A Thesis Submitted to the

Graduate School of Natural and Applied Sciences of

Ankara Yildirim Beyazit University

In Partial Fulfillment of the Requirements for the Degree of Master of Department of Defense Technologies

by

Mehmet Emin ERCAN

May, 2022

ANKARA

M.Sc THESIS EXAMINATION RESULT FORM

We have read the thesis entitled **“INVESTIGATION OF ADHESIVELY-BONDED JOINTS FOR AEROSPACE AND AUTOMOTIVE INDUSTRIES”** completed by **MEHMET EMİN ERCAN** under supervision of **PROF. DR. FERHAT KADIOĞLU** and we certify that in our opinion it is fully adequate, in scope and in quality, as a thesis for the degree of Master of Science.

Prof. Dr. Ferhat KADIOĞLU

Supervisor

Assoc. Prof. Dr. Mustafa KAYA

Jury Member

Assist Prof. Dr. Mohamed Salem ELMNEFI

Jury Member

Prof. Dr. Sadettin ORHAN

Director

Graduate School of Natural and Applied Sciences

ETHICAL DECLARATION

I hereby declare that, in this thesis which has been prepared in accordance with the Thesis Writing Manual of Graduate School of Natural and Applied Sciences,

- All data, information and documents are obtained in the framework of academic and ethical rules,
- All information, documents and assessments are presented in accordance with scientific ethics and morals,
- All the materials that have been utilized are fully cited and referenced,
- No change has been made on the utilized materials,
- All the works presented are original,

and in any contrary case of above statements, I accept to renounce all my legal rights.

Date: 2022, 10 May **Signature: ……………………………………**

Name& Surname: Mehmet Emin ERCAN

ACKNOWLEDGMENTS

On this occasion, I would like to thank my teacher and advisor Prof. Dr. Ferhat Kadıoğlu for the support, guidance, encouragement and enthusiasm he showed as an older brother rather than a consultant from the beginning to the end of the project. It was an honor and pleasure to work with him.

I would also like to express my gratitude to Assoc. Prof. Dr. Mustafa KAYA for his support and guidance.

I would like to thank to my wife, mom and dad, for being with me all the way. And finally, I would like to thank my little daughter for showing me her smiling face even when I wanted to spend it with her and couldn't.

Without all of you, I wouldn’t be here.

2022, May **Mehmet Emin ERCAN**

INVESTIGATION OF ADHESIVELY-BONDED JOINTS FOR AEROSPACE AND AUTOMOTIVE INDUSTRIES

ABSTRACT

This thesis aims to investigate the effect of different bonding lengths under the effect of high-speed collision. Within the scope of the study, the effect of the collision on the single lap joint on the static strength was investigated. To gain a better understanding of the dynamic behavior specific to overlay joints, a series of quasi-static experiments have been performed on lap joints. In this context, carbon and glass fiber adherent joints were subjected to tensile and bending tests to obtain information about the static joint behavior. Then, while starting the ballistic tests, firstly, due to the similar reaction to the impact, vibration studies were carried out on the composite joints and information about the natural frequency of the material and the measurement technique was obtained. In the ballistic experiments, samples of AL6061 aluminum bonding elements with 15mm and 25mm length single lap joints were produced by using AF163-2K film adhesives used in aviation. An air-pressure rifle was positioned on a uniquely designed shooting range, and shots were made with the laser pointer. The bullets leaving the rifle and going to the target were recorded with a fast camera and their approximate speeds were determined. At the same time, models were obtained in the Abaqus FEA program. In the light of the results obtained from numerical analysis and experiments, the change in strength caused by the collision on the overlap length has been interpreted.

Keywords: High-velocity impact, adhesively bonded joints, air pressurized gun, finite element method.

OTOMOTİV VE HAVACILIKTA KULLANILAN YAPIŞTIRMALI BAĞLANTILARIN ARAŞTIRILMASI

ÖZ

Bu çalışmanın amacı yüksek hızlı çarpışma etkisi altında farklı yapıştırma uzunluklarında meydana gelen etkinin araştırılmasıdır. Çalışma kapsamında tekli bindirme bağlantısı üzerine etki eden çarpışmanın statik mukavemet üzerindeki etkisi araştırılmıştır. Bindirme bağlantılarına özgü dinamik davranışın daha iyi anlaşılması için, bindirme bağlantıları üzerinde bir dizi statik yarı-statik deneyler yapılmıştır. Bu bağlamda karbon ve cam fiberden üretilmiş eklemler çekme ve eğme deneylerine tabi tutularak statik bağlantı davranışı hakkında bilgi edinilmiştir. Daha sonra balistik testlere başlarken, öncelikle temelde etkiye karşı benzer tepki göstermesi sebebiyle, kompozit eklemler üzerinde titreşim çalışması yürütülerek malzeme doğal frekansı ve ölçüm tekniği hakkında bilgi edinilmiştir. Balistik deneylerde havacılıkta kullanılan AF163-2K film yapıştırıcılar kullanılarak AL6061 alüminyum yapıştırma elemanları ile 15mm ve 25mm uzunluklu tekli bindirme bağlantıları oluşturulmuş numuneler üretildi. Hava basınçlı bir tüfek, özgün tasarımlı bir atış poligonuna konumlandırılarak lazer noktalama ile atışlar yapılmıştır. Tüfekten çıkarak hedefe giden kurşunlar, hızlı kamera ile görüntülenerek yaklaşık hızları tespit edilmiştir. Aynı zamanda Abaqus FEA programında modeller elde edilmiştir. Nümerik analiz ve deneylerden elde edilen sonuçlar ışığında bindirme uzunluğu üzerinde çarpışmanın meydana getirdiği mukavemet değişimi yorumlanmıştır.

Anahtar Kelimeler: Yüksek hızlı çarpışma, yapıştırmalı bağlantılar, hava basınçlı tabanca, sonlu elemanlar metodu.

CONTENTS

NOMENCLATURE

$\dot{\bar{\varepsilon}}_p$	Effective Plastic Strain Rate
$\dot{\varepsilon}_0$	User Defined Refence Plastic Strain Rate (normally Taken as 1/s)
$\bar{\varepsilon}_p$	Effective plastic strain
G_{fc}	Fracture Energy for Longitudinal Compressive
G_{ft}	Fracture Energy for Longitudinal Tensile
G_{mc}	Fracture Energy for Transverse Compressive
G_{mt}	Fracture Energy for Transverse Tensile
σ_{12}^u	Shear (1,2)
σ_{1C}^u	Longitudinal Compressive (1)
σ_{1T}^u	Longitudinal Tensile (1)
σ_{23}^u	Shear (2,3)
σ_{2C}^u	TransverseCompressive (23)
σ_{2T}^u	Transverse Tensile (23)
A	Initial Yield Stress
AIAA	American Institute of Aeronautics and Astronautics
B	Strain Hardening
C	Strain Rate Coefficent
CCCM	Carbon-Carbon Composite Materials
CMC	Ceramic Matrix Composite
E_{11}	Elasticity modulus for X direction
E_{22}	Elasticity modulus for Y direction
f1	Tensile fiber failure Criterion
f2	Compressive fiber failure criterion
f3	Tensile matrix failure criterion
f4	Compressive matrix failure criterion
G	Shear Modulus
J-C	Johnson-Cook
MMC	Metal Matrix Composites
n	Strain Hardening Exponent
PMC	polymer matrix composite
SDC	Specific Damping Capasity

SHPB	Split Hopkinson Pressure Bar
SLJ	Single Lap Joints
SSJ	Single Strap Joints
Tm	Melting Temperature
Tr	Room Temperature
V	Poison Ratio

LIST OF TABLES

LIST OF FIGURES

CHAPTER 1

INTRODUCTION

Industrial development, which started with the industrial revolution in history, has brought about a dizzying progress in the aviation and space industry during the last century. Scientists in the scientific and technical field have made important discoveries with their research. Even though all these developments and researches on defense and military fields are carried out by countries, they have pioneered seminal changes for the products in many industrial branches today.

Composite materials, which have left their mark especially in the last forty years, have been continuously researched and their usage areas have increased since the first day they started to attract attention with their lightness and strength. As such, it shows that composite materials will continue to find a place for itself in many areas. Composite materials, which have been used in many branches of the industry, have started to replace heavy iron-steel constructions, and have been the pioneer of the change in mechanical joints used for machine parts to come together and form a whole. For example, resins used in fibrous composite materials to keep the fibers together and to provide fiber resistance are different types of adhesives. On the other hand, the strength properties of composite materials are provided by fibers to a significant extent. Therefore, continuity in the internal structure of the material is very important. In order to use fasteners such as bolts and rivets in assembly, it is necessary to drill holes that disrupt the fiber continuity and create a notch effect. Adhesives eliminate this handicap by providing material continuity. The more important the mechanical properties of the parts for construction strength are, the more important the performance of the fasteners for the joints are. For example, the damage to the main parts or fasteners of a machine produced for use in fields such as defence, automotive and aerospace during its use in the field may not cause financial damage at the same rate, but it can be equally deadly in terms of its results.

1.1 Literature Review

While the use of composite materials is expanding day by day because of the advantages they provide, many researches and publications related to composite materials have been made and are being made. Academic researches have been published on the classification, production methods, test methods, mechanical properties, damage criteria, connection methods and many other subjects of composite materials. In this part of the study, we will review various studies on composite joints and joint damage.

As it is known, one of the main reasons for weak joint strength and stress concentration formation is material geometry. Rivet or screw holes in the connection area are important factors that reduce the strength. [1,2] When examined in detail, it is seen that many factors affecting the geometry also affect the joint strength. [3] In addition to these, it is seen that the connections show different mechanical performance under different loading conditions applied to the connection. [4,5] The decrease in strength that occurs with the increase of adhesive thickness in adhesive connections is also seen in the studies in the literature. [6,7] A uniform stress distribution is desirable when designing the joint. However, ideal connection cannot be achieved due to many reasons such as eccentric loading conditions, geometric material discontinuity. Many researchers have tried to overcome these problems by the methods they have found. [8-11] In the numerous studies on the bonding joints of laminated composite materials, two very important factors stand out: one of them is the fiber orientation of the bonded composites. It has been observed that the load carrying capacity of the link increases with decreasing fiber orientation. Another important factor is the overlap length. Increasing the overlap length increases the mechanical performance of the joint. [12-15] Araújo et al. numerically modeled the quasi-static and dynamic test results obtained in their studies. The obtained results were compatible with the numerical model. [16] Takeda et al., on the other hand, made applications to increase fracture toughness between layers by using additive agents. When they compared their experimental observations with the analytical model, they saw that the results were consistent. [17] In another study on adhesive bonds, Lapczyk et al. studied fracture toughness and bond strength. In the study in which a damage model is presented, issues such as damage convergence and network sensitivity are also discussed by using the finite element code while the damage process is being studied. [18]

Today, ballistic performance of materials, which is a very new research area, emerges as a complex problem that needs to be solved in material strength. Although ballistic material behavior has been extensively studied in the last four decades, it is a relatively new field of research. When we look at the literature, it is immediately apparent that considering the material behavior dynamically is more complex than looking at it statically. Yokoyama in 2003 measured the effect of loading rate on lap joints made with different adhesives. As a result of the study, it was stated that there is an optimum adhesive thickness for lap joints. [19]

Rashed et al. carried out a numerical analysis on the behavior of different materials used in multilayer alumina ceramic composite armors under ballistic conditions. Many cases such as bullet interaction time, bullet velocity variation and bullet erosion during the collision were investigated. [20]

Kelly investigated the load-bearing properties of hybrid metal connections in his research in 2004. The load distributions and connection behavior were investigated by comparing the finite analysis model created by using boundary conditions and the experimental studies [21].

Bois et al., on the other hand, tried to confirm the damage estimates with experimental results by presenting an analytical model proposal for hybrid lap joints that they developed using multiple strength criteria [22].

Chan and Vedhagiri compared their experimental work with the finite element model to understand and predict the structural responses of various single thrust and hybrid joints under load in laminated composite materials and conducted a parametric study on the stress distribution and load transfer effects resulting from the array [23].

Meyer et al., in their study on the impact mechanics strength of composite materials in 2018, made a research on the damage conditions and material behavior under ballistic effect in thin composite layers by using high-speed imaging technique. The resistance of single-layer composites to the piercing effect has been investigated [24].

Bonyi et al., in their study in 2018, transferred the imaging data obtained from ballistic tests to the Matlab program and produced damage maps on the material. They analyzed the characteristic behavior by interpreting the damage patterns on the material [25].

Yaghoubi et al. made a experimental verification by comparing the numerical model they established with the ballistic tests they performed on aluminum sandwich specimens glued together with the help of composite laminates. They also interpreted the puncture patterns obtained from the experiments and studied damage mechanics [26].

Sevkat et all studied the damage to composite beams subjected to ballistic impact by using a high-velocity gas gun. They examined percent elongation which occured due to collision with the strain gauges placed on the composite specimens. They verified the experimental results with the 3D dynamic nonlinear finite element model [27].

Holmquist et al. studied the characterization and modeling of the (ARL) 14.5 mm BS41 projectile for ballistic impact conditions. The ARL BS41 is a complex projectile which include a steel casing, inert fillers, and an armor-piercing tungsten carbide (WC) core. They presented an approach to determine the Johnson-Cook strength and fracture numerical model constants for the WC core by using ballistic impact test data [28].

Aviral Shrot and Martin Bäker tried to find a method for the reverse definition of Johnson Cook parameters. Using a specific set of Johnson-Cook parameters to describe the material behavior, they constructed an idealized finite element model for high-speed machining that conforms to the specified parameters for the process [29].

Nitin Thakur et al., in their experimental study on a material they determined, made numerical model comparisons with the experiments. In the study, they found that D3 was the most sensitive in terms of material behavior among the hard-to-find Johnson-Cook material parameters [30].

Xuemei Wang and Jun Shi 2, in their study in 2013, found compatibility in the dimensions of the crater opened on the material in the results of their experimental studies and numerical analysis with a high-speed ball thrown at different angles and speeds on the Ti-6Al-4V material [31].

Mahmood M. Shokrieh et al., in a study they conducted in 2016, investigated the behavior of carbon nanofiber-epoxy composite materials depending on the deformation rate. For this purpose, they compared the results obtained from the tensile and shear tests with the numerical results by using the modified Johnson-cook material model [32].

Kenneth Gollins and others applied crash tests to different adhesives in their work in 2020. They tried to determine the behavior characterization of materials at high strain rates under dynamic loading conditions with their original method.[34]

Tamrakar et al. observed the change of material strength at different strain rates depending on temperature. For this purpose, they used split Hopkinson Pressure bar and universal tensile test devices. Experimentally obtained data showed compatibility with computer-aided simulation models.[35]

When the literature is examined, the researchers discussed the behavior of hybrid joints made with composites and joints obtained by bonding metalic materials, under quasi-static and high strain conditions, depending on the overlap length, adhesive thickness and adherend thickness. It is seen that researchers mostly simulate the tests with various experimental setups by modeling them in three dimensions, using the finite element analysis method, and comparing the test results with the simulation results. In this study, composite-composite and metal-metal single lap joints were subjected to static and dynamic tests in the laboratory environment. Numerical models (36) established by using the Abaqus library with the Abaqus CAE package program were used to estimate the data obtained from the experiments.

The most commonly used test methods for structural adhesives and/or adhesive joints under high loading rates are pendulums, drop weight impactors and split Hopkinson pressure bars as seen from the literature view. In structural applications, adhesives are preferably loaded in the shear mode so that the best joint performance can be achieved.

CHAPTER 2

COMPOSITE MATERIALS

2.1 Definition

Although they are not recognized differently in the literature, composite materials, in the most general definition, are materials that have different physical properties from the characteristics of materials when at least two materials with different chemical and physical properties come together at a macro level.[37] Generally, fibers with high modulus and high strength adhere to each other in accordance with the interfacial bonding properties with the matrix material. Composite materials are multi-functional materials that can be prepared in accordance with the desired application area. Mostly, it is the product of the desired strength to be obtained with the cheapest cost and the lowest weight expected from the combination.

2.2 General Features

A composite material consists of a reinforcing material that provides the composite rigidity and a matrix material that wraps around this material and holds and protects the reinforcing material. By using the known properties of the components that make up the composite material, some properties of the material such as density, elastic modulus, tensile strength, weight ratio-volume ratio conversion can be calculated. When the appropriate matrix and suitable reinforcement material are selected, it may be possible to produce the desired composite material.

Composite materials can be composed of many different materials. These combinations of compounds are almost limitless. We can add almost any natural or synthetic material to the composition according to the desired properties. Since each ratio of this composition will enable us to obtain materials with different properties, the product variety is also endless. For this reason, depending on the need, the composite material we will obtain can be provided with the following many features;

-High strength

-High rigidity

-High fatigue strength

-Good wear and corrosion resistance

-High thermal capacity

-Thermal and electrical conductivity

-Low density

-Good surface quality.

Composite materials cannot provide all of these properties at the same time. However, the required properties can be optimized by combining the matrix and reinforcement material to be selected at a certain rate.

2.3 Classification of Composite Materials

Composite materials can be classified in many ways according to the physical, chemical structure and properties of the matrix and reinforcement materials that form it. Since composite materials consist of two main components, reinforcement and matrix material, they are expressed in two classifications in the general classification.

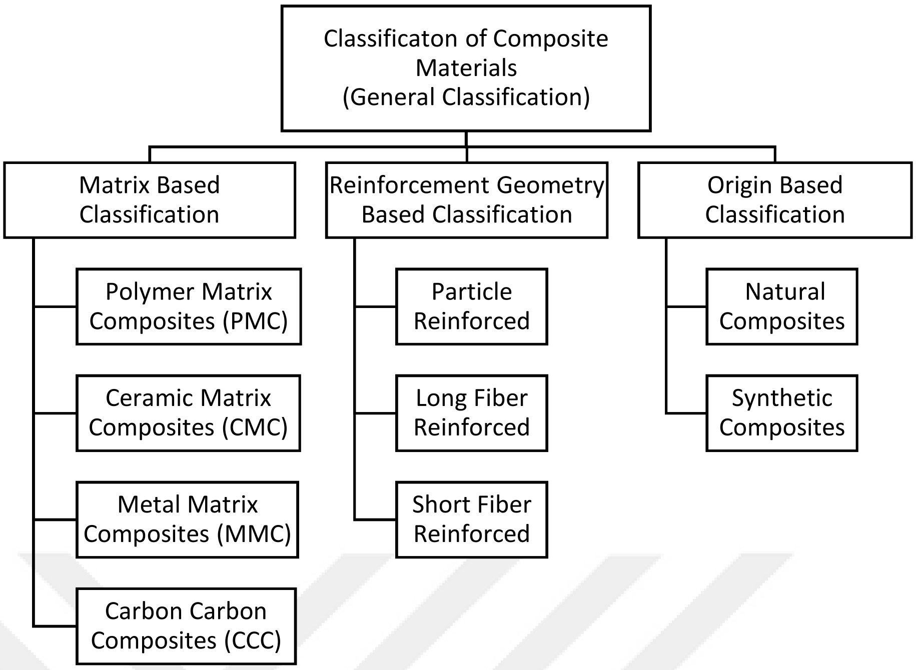

Figure 2.1 Classification of Composite Materials

According to the matrix material, they are called polymer matrix composites (PMC), ceramic matrix composites (CMC), metal matrix composites and carbon-carbon composites. According to the reinforcement material, they are classified as particle reinforced composites, short fiber reinforced composites, and long fiber reinforced composites. In classification according to their origin, they are divided into natural and synthetic composites. (Figure 2.1). [39]

2.3.1 Classification of Composite Materials by Matrix Material

2.3.1.1 Polymer Matrix Composites (PMC)

The use of polymers as matrix material is the most common form of use in composite materials. They are generally used by reinforcing with fibers. The stiffness and fracture toughness of polymer matrix composites are quite high. They have high resistance to abrasion, puncture and corrosion. However, since PMC's is highly sensitive to temperature, its mechanical properties decrease significantly with temperature increases. High coefficients of thermal expansion are important disadvantages.

2.3.1.2 Metal Matrix Composites (MMC)

As the name suggests, MMC's are composite materials that use metal as matrix material. Alloys of metal elements such as aluminum, magnesium, titanium and copper with low density are used as matrix material. Operating temperatures can be up to 4-5 times higher than polymer matrices on the selsius scale. Therefore, it is more preferred in high temperature applications. They have high ductility, mechanical strength and stiffness properties. However, it is costly and difficult to process.

2.3.1.3 Ceramic Matrix Composites (CMC)

Ceramics are structural materials with high temperature resistance that define a wide range of materials. It has high elastic modulus value, high static and shear strength. Since it is a very hard and stable material, it has high brittleness and low impact resistance.

2.3.1.4 Carbon-Carbon Composite Materials (CCCM)

CCCM's are composite materials in which both the matrix and the reinforcing material are carbon. It is a very hard and very durable material, as it consists entirely of carbon. It is obtained by applying a series of processes by heating a carbon preform matrix to 3000 degrees.

2.3.2 Classification of Composite Materials According to Reinforcement Geometry

2.3.2.1 Particle-Reinforced Composite Materials

Particle-reinforced composites, which we can also call filled composites, are made by adding particle reinforcement into the matrix material, from nano sizes to macro sizes, according to the desired property. Here, the better the adhesion between the filler material and the matrix material, the less moisture retention and the higher the mechanical strength of the composite material. The material exhibits approximately the same behavior in space in all three directions.

2.3.2.2 Long fiber reinforced composites

Continuous fiber composites are the most effective reinforcements. They stretch and relax together with the matrix material in the fiber direction and show a complex stress-strain curve. The strength curve of the composite material is between the strength curve of the matrix material and the fiber material, depending on the mixing ratio and it changes in this range. Fibers that can show strength in two and three dimensions can be produced with various weaving techniques used in textiles. In this study, long fiber composite materials used for the investigation.

2.3.2.3 Short Fiber Reinforced Composites

In order to talk about the presence of fibers in discontinuous fiber composites, the fibers must be long or equal to a critical fiber length value (lc). This length is a calculated value based on the fiber diameter, the fiber-matrix interface shear stress, and the fiber tensile strength value. Fibers are considered as continuous fiber when the fiber length is approximately 15 times longer than this critical value.

2.3.3 Fiber Orientation Effect

In composites with continuous fibers, we can mention that the fibers do not have a regular arrangement or there is little, but there is a regular orientation in continuous fiber composites under normal conditions. As the fiber angle starts to increase relative to the force axis, the strength values of the composite material begin to decrease. [40]

CHAPTER 3

IMPACT METHOD

3.1 Definition

Impact mechanics is one of the most challenging branch of engineering mechanics required for civil, military and scientific applications. A ballistic-grade dynamics problem requires a detailed consideration of its experimental observations and, if any, the underlying theory. Impact mechanics encompasses a broad subject where research has been undertaken to understand transient loads, industrial accidents and explosions that produce high strain rates. Impact-induced stress waves occur, which propagate through high-speed deformation under the effect of impact. The motion of waves is felt everywhere, as in the case of earthquakes, tsunamis, and explosions.[53] On the other hand, estimating action-response and damage in collision mechanics requires extensive material modeling that includes variables like strain rate, temperature etc.

3.2 Investigation Methods

In machinery, a component is expected to provide the required performance under the operating conditions at the place of use. In order to prevent the said before component from causing an accident or being damaged, it is subjected to tests according to the working conditions. Since the materials exhibit behavior differences according to the deformation rates, the test speed affects the damage case of the material. Therefore, many test methods have been developed depending on the strain rate. Some of the most well-known methods are listed in this section. [51-55]

3.2.1 Quasi Static Material Test

Tensile or compressive testing of a material is a common standard technique that can be used by all researchers and students to determine material properties under static and quasi-static conditions. Quasi-static tests are performed using a test device in which the specimen is crushed or pulled at very low crosshead speed between two parallel jaws. The energy absorption capacity of velocity sensitive materials depends on the strain rate. Therefore, a quasi-static test does not give an exact conclusion about the crash-proofness of a structure, as it can be seen as almost static [51-53]. (Fig. 3.1)

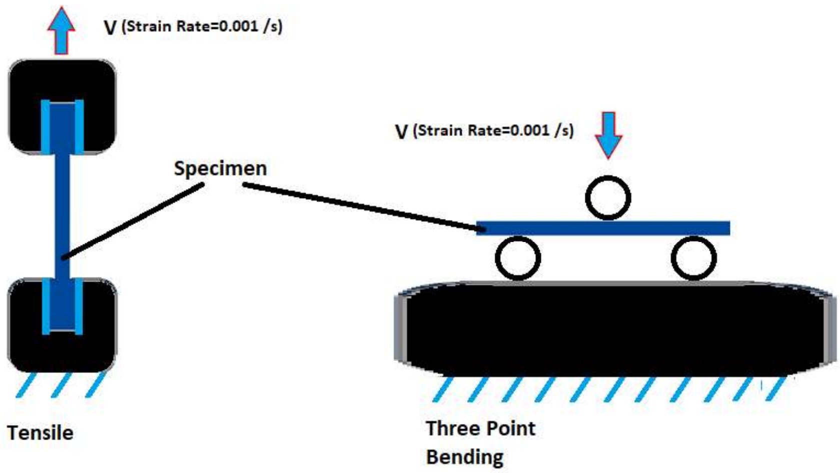

Figure 3.1: Quasi-Static Test Conditions

3.2.2 Pendulum Test

Pendulum impact tests are applied to understand the energy absorption properties of a material under certain ambient conditions before it breaks when subjected to a sudden applied load.

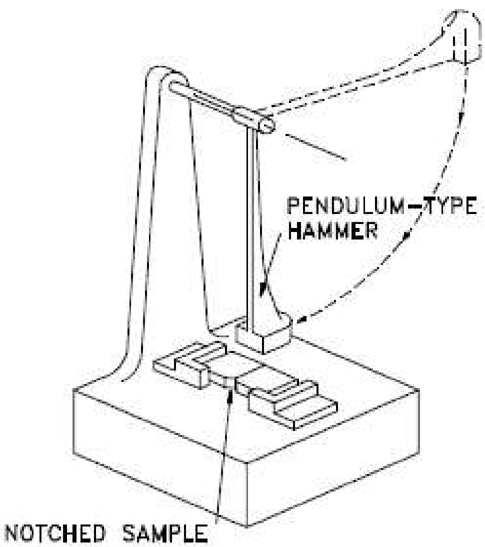

Figure 3.2 Charpy Impact Test

The strain rate applied to the specimen is possible to be between 1 s-1 and 1000 s-1 depending on the design and size of the pendulum impact machine [51-53]. These tests are mostly known as Izod and Charpy Impact Tests in the literature. The Charpy Impact test set-up has shown in Fig 3.2.[57]

3.2.3 Drop Test

Although there are many types, we can collectively examine drop tests in two groups as sample drop tests and weight drop tests (Fig. 3.3). In drop tests, which are used to measure the durability of commercial products that could be damaged during an accident, drop, or transportation, samples are released into free fall from a distance. On the other hand, with the test setup set up usually in cases where the gravitational acceleration is basis to create an impact load is collided with the sample by placing a certain weight from a certain distance. These cases can be evaluated by the actual tests within the laboratories before the finalization of the design [53].

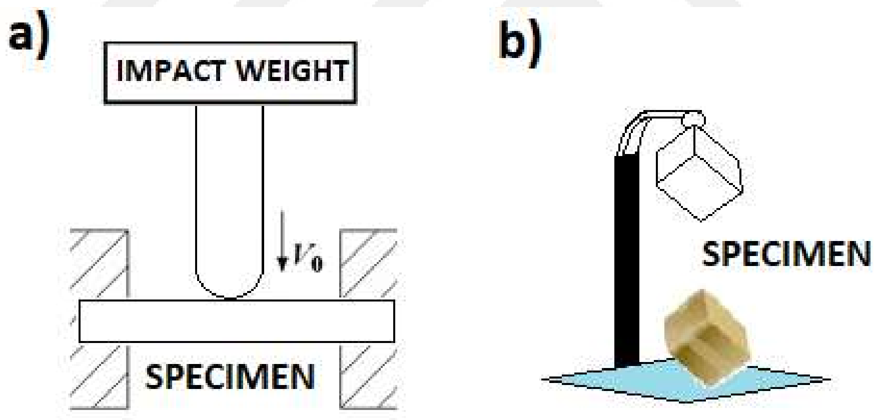

Figure 3.3 Example schematics of weight drop (a) test and sample drop (b) test.

3.2.4 Tylor Cylinder Impact Test

The Taylor impact test, also known as Taylor cylinder test or Taylor anvil test, is a simple and cheap impact method. The Taylor impact test is defined as a cylindrical specimen is accelerated to strike a hard target with 90 degree angle to become deformation. Taylor impact tests are performed using a gas gun to launch rod samples.

The impact deforms the sample plastically and it becomes a shorter and wider shape. Fig 3.4 shows a test facilty anda test sample.[53-55]

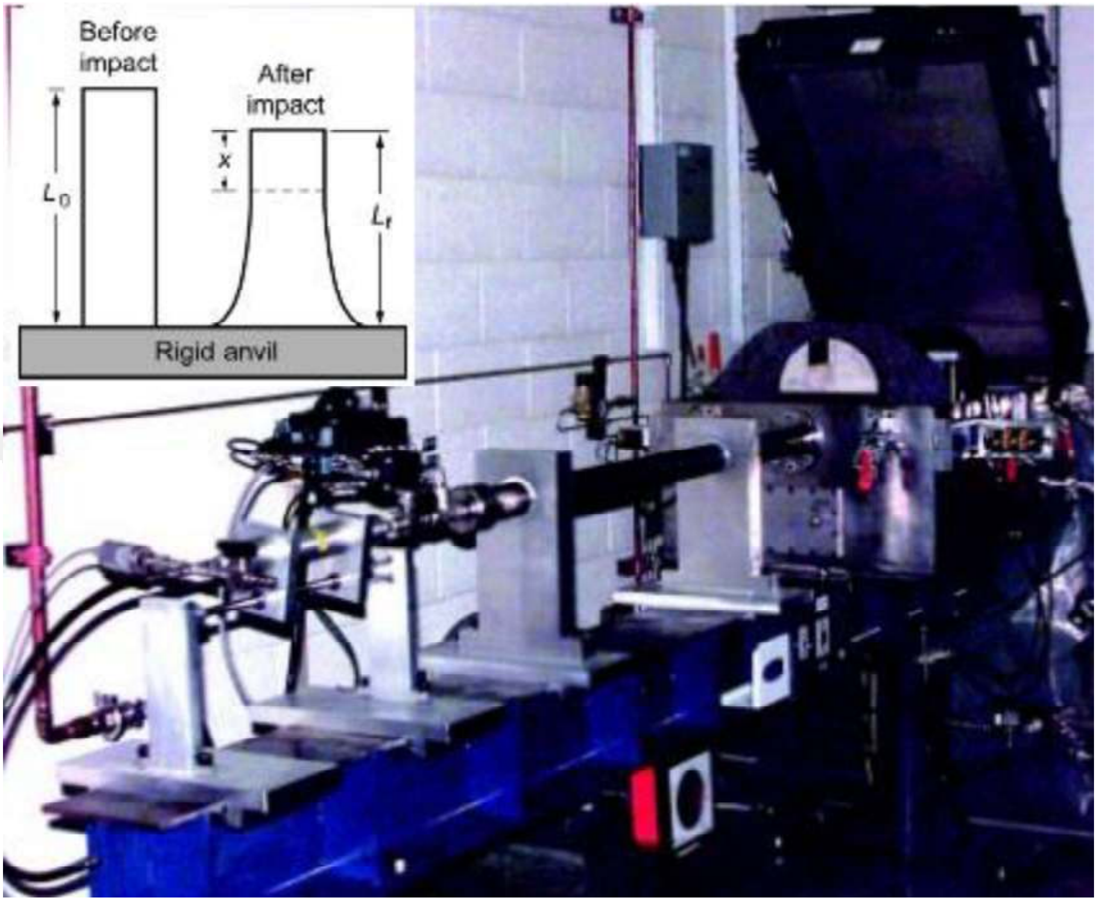

Figure 3.4 A Taylor cylinder impact test facility and a test sample

3.2.5 Half Power Bandwith Vibration Test Method

For current work, this test method has been clarified since it is thought that there is a correlation between the damage and vibration in the samples tested under ballistic conditions. To examine the resonance frequency of the beam, the following equation is used, in which the elastic modulus, dimensions and density are used.[59]

$$f_n = \frac{1}{2\pi}\left(\frac{\lambda_n}{l}\right)^2\sqrt{\frac{EI}{\rho t b}} \qquad \textbf{(3.1)}$$

Where;

- λn = Eigenvalues for clamped-free end conditions,

- n = mode number,
- E = flexural modulus,
- I= the second moment of area,
- l= the length of the beam,
- ρ= the mass density.
- t= the thickness,
- b= the width of the beam,
- EI= the flexural rigidity

3.2.6 Split Hopkinson Pressure Bar Test (SHPB)

This test is applied to understand material behavior under strain rates ranging from 100 /s to 10000 /s. This technique, used to measure the shape of an impact stress pulse on a long elastic rod, was first described by Bertram Hopkinson in England in 1914. Afterwards, many researchers made improvements and tried to get clearer and more accurate data.

There are various setups and techniques currently in use for the SHPB test and operation. There is no universal standard design for the SHPB apparatus. However, the underlying principles for the test and measurement are the same and all SHPB apparatus share common design elements such as:

- Air cannon/compressed gas gun that fires a projectile;
- Sensing device to determine the projectiles velocity;
- Two long symmetric pressure bars;
- Bearings and alignment tooling to allow the pressure bars to move freely;
- Strain gauges mounted on both pressure bars;
- Test specimen; and instrumentation to record stress, strain, and strain rate information.

Besides a concept design of the test method has shown in Fig.3.5. [53]

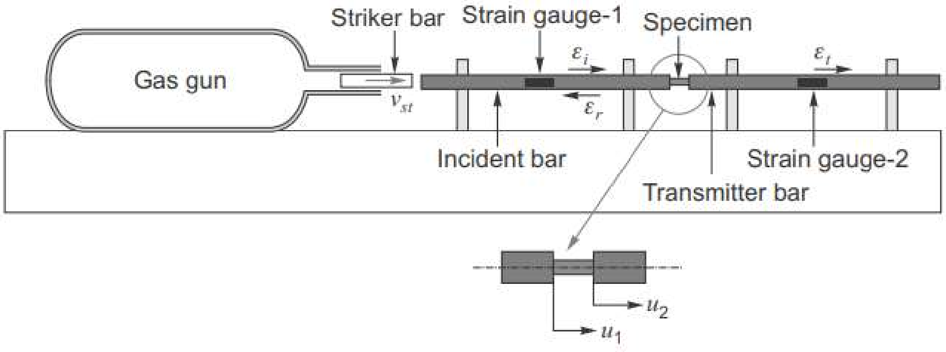

Figure 3.5 A SHPB concept test design.

3.2.7 Johnson-Cook Numerical Model

The Johnson-Cook (J-C) model was introduced by johnson and Cook in 1983. It was primarily intended for computational work and the mathematical model was formulated by gathering test data at different strain rates and temperatures for a wide range of test procedures. Johnson and Cook material model is an empirical constitutive model for metals. It is described as strain rate and adiabatic assumed temperature-dependent visco-plastic material model.

This model is suitable for problems where strain rates vary over a large range and temperature change due to plastic dissipation causes material softening. This model describes higly dynamic problems, large strains, and high temperature change cases of metallic materials. For each of strain hardening and thermal softening, an independent term is created. Due to the constitutive model is relatively easy to calibrate since and allows isolation of the various effects , the model is frequently used in the ballistic

investigations. The yield stress is given by the following expressions in formula:[53]

$$\sigma_y = [A + B\bar{\varepsilon}_p^n][Cln\left(\frac{\dot{\bar{\varepsilon}}_p}{\dot{\varepsilon}_0}\right)][1 - (\frac{T-T_r}{T_m-T_r})^m] \quad \textbf{(3.2)}$$

Where;

- A: initial Yield Stress

- B: Strain Hardening
- n: Strain Hardening Exponent
- $\dot{\bar{\varepsilon}}_p$: Effective Plastic Strain Rate
- $\bar{\varepsilon}_p$: Effective plastic strain
- $\dot{\varepsilon}_0$: User Defined Refence Plastic Strain Rate (normally Taken as 1/s)
- C: Strain Rate Coefficent
- Tr: Room Temperature
- Tm: Melting Temperature

3.3 Methodology of the Study.

The work plan of thesis illustrated in Fig. 3.2. Manufacturing, tests and numerical analysis will be performed as shown. Firstly, composite-composite joint specimens will be examined under quasi-static conditions tensile and bending tests will be performed. The purpose of these tests is to understand the stress and damage behavior of composite joints with different orientations and material properties under bending and tensile loads. In the second stage, single strap joints will be tested and the relationship between vibration, composite and orientation angle will be investigated. Finally, the relationship between damage and vibration in lap joints under impact conditions will be examined.

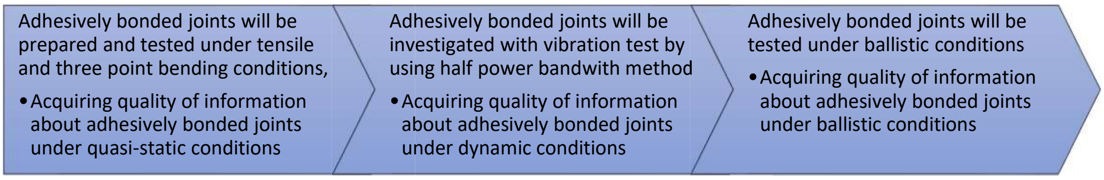

Figure 3.6 Work plan of the Thesis.

CHAPTER 4

INVESTIGATION OF JOINT MECHANICS WITH COMPOSITE TO COMPOSITE BONDED JOINTS

4.1 Tensile and Flexural Mechanics in Carbon Fiber Composites

Scientific studies in this section have been published by the American Institute of Aeronautics and Astronautics (AIAA) in 2018. The works done in this study are supported by the Turkish Aerospace Industry.

4.1.1 Aim of The Study

The aim the Works carried on in this saction is to investigate quasi-static performance of adhesively-bonded joints manufactured with adherends with laminated glass fiber composite materials that have different orintations under tensile and bending loading modes.

4.1.2 Materials Used

The materials used in this study are an adhesive film, AF163 2K produced by 3M, and adherends, manufactured from a glass reinforced polymer matrix composite, Hexply 913/33%/UD280, produced by Hexcel. While the adhesive used was cured at 125°C for 60 minutes under a pressure of 2 bars, the cure procedure for the prepreg of the composite adherends was 130°C for 120 minutes under a pressure of 5 bars. All the joints were manufactured using a specially designed mould in which the specimens were allowed to be manufactured with different adherend thicknesses and different overlap lengths.

In addition, computer-aided simulation method was used for the interpretation of the results, and the material properties used for numerical modeling are shown in Table 4.1 [42].

Table 4.1 Mechanical Properties of Glass Fiber Composite & Adhesive Layer

		Parameter	Symbol	Value
Adherent	Strength (MPa)	Longitudinal Tensile (1)	σ_{1T}^{u}	1200
		Longitudinal Compressive (1)	σ_{1C}^{u}	850
		Transverse Tensile (2,3)	σ_{2T}^{u}	70
		TransverseCompressive (2,3)	σ_{2C}^{u}	90
		Shear (1,2)	σ_{12}^{u}	95
		Shear (2,3)	σ_{23}^{u}	50
	Damage (J/mm^2)	Fracture Energy for Longitudinal Tensile	G_{ft}	10
		Fracture Energy for Longitudinal Compressive	G_{fc}	10
		Fracture Energy for Transverse Tensile	G_{mt}	2.5
		Fracture Energy for Transverse Compressive	G_{mc}	2.5

E_{11}	E_{22}	V_{12}	G_{12}	G_{13}	G_{23}
44000	13000	0.2637	6900	6900	6200

	True Stress (MPa)	True Strain
Adhesive	15.0349676	0
	16.5889964	0.0014815
	18.1847065	0.0014815
	20.4960152	0.00261002
	23.4960152	0.00410646
	26.3381828	0.00560067
	28.9810794	0.00711041
	30.265838	0.00791915
	32.6707453	0.00943031
	36.4827251	0.01205514
	40.1311388	0.0151019
	43.606809	0.01898998
	46.1848655	0.0230009
	47.8340181	0.02673

E_{11}	v
2300	0.3

Where; E_{11} and E_{22} are elasticity modulus elong the X and Y directions respectively, v is poisson ratio G is the shear modulus of the indicated plane.

4.1.3 Experimental Works

In the current work, a series of experimental studies were conducted. While the thickness of the adherends and the adhesive layer were kept constant, 2 mm and 0.200 mm, respectively, the composite adherends with 10 layers for different fiber orientations - 10°, 20°, 45° and 55° (symmetric and balanced) – and for different overlap lengths, 15 mm, 25 mm and 40 mm, were considered. Dimensional details of the tested samples are shown in Figure 4.1.

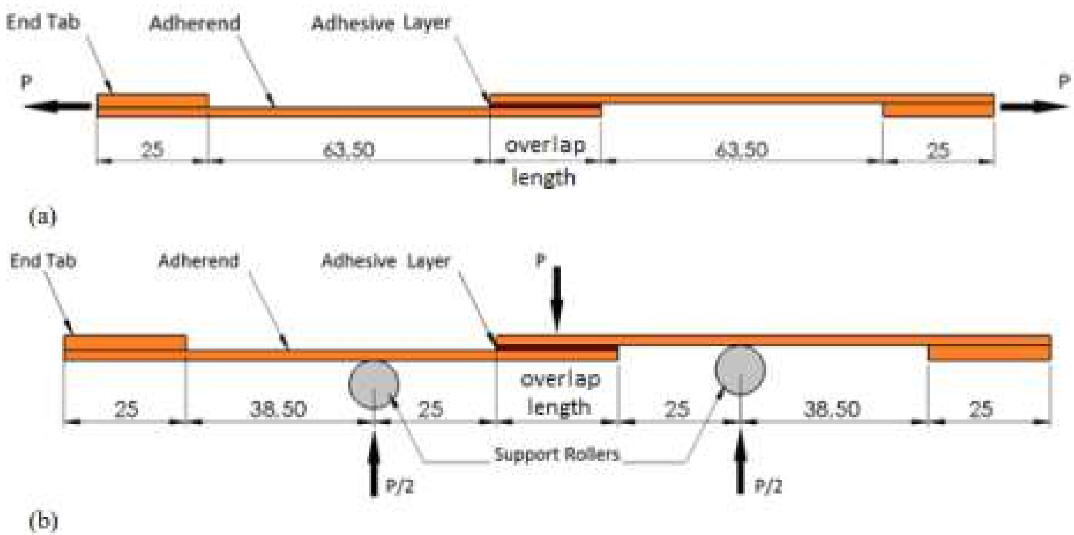

Figure 4.1 Geometrical details of the tested samples a) tensile b) bending

4.1.4 Numerical Works

Numerical analysis was run to understand the joint mechanical performance for different loading modes using the ABAQUS/Standard finite element program. 4 different fiber orientations(10°, 20°, 45° and 55°) and three different overlap lengths (15mm, 25mm and 40mm) were considered. In both models, under tensile and bending loading, the composite adherents and adhesive layer were discretized with 8-node quadrilateral in-plane continuum shell (SC8R) elements and 8-node linear brick (C3D8R) elements respectively.

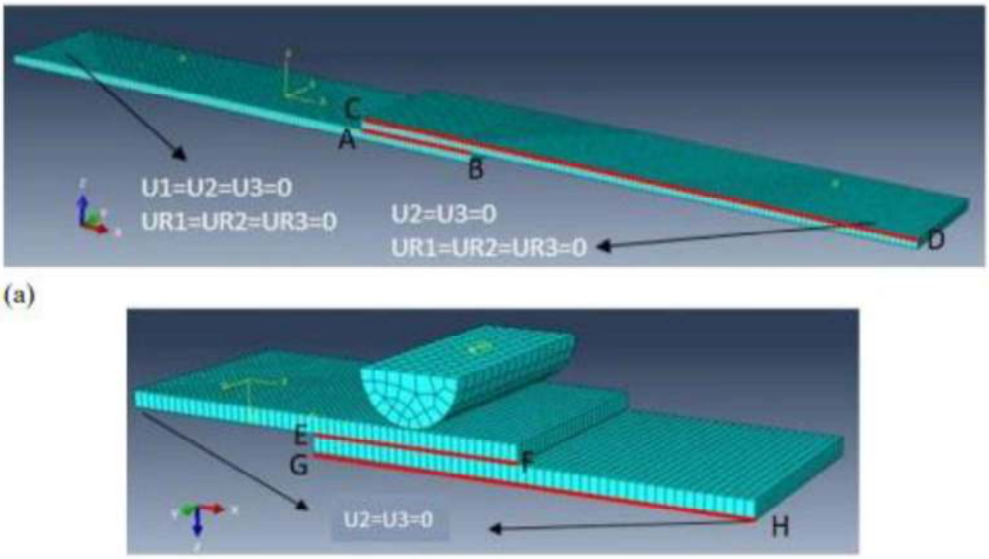

(a)

(b)

Figure 4.2 Meshing and boundary conditions for the joint under tensile (a) and bending (b) loading.

The boundary conditions for the specimen under tensile loading are shown in Fig. 4.2 (a); one side was fixed, and the other side was allowed to move along the tensile loading direction. For the bending case, the boundary conditions are shown in Fig. 4.2(b); both right and left hand sides of the model were restricted in the y and z directions, where the support rollers are located, and a displacement was applied on the top side of the half cylinder.

4.1.5 Results

In this part of the work, primarily, experimentally and numerically obtained maximum loads from tensile and three point bending loading modes for the composite adherends with 10°, 20°, 45° and 55° fiber orientations, were presented, for 15mm overlap length. These experimental and numerical results, which show good agreement, are shown in figures 4.3(a) and 4.3(b) for tensile and bending, respectively.

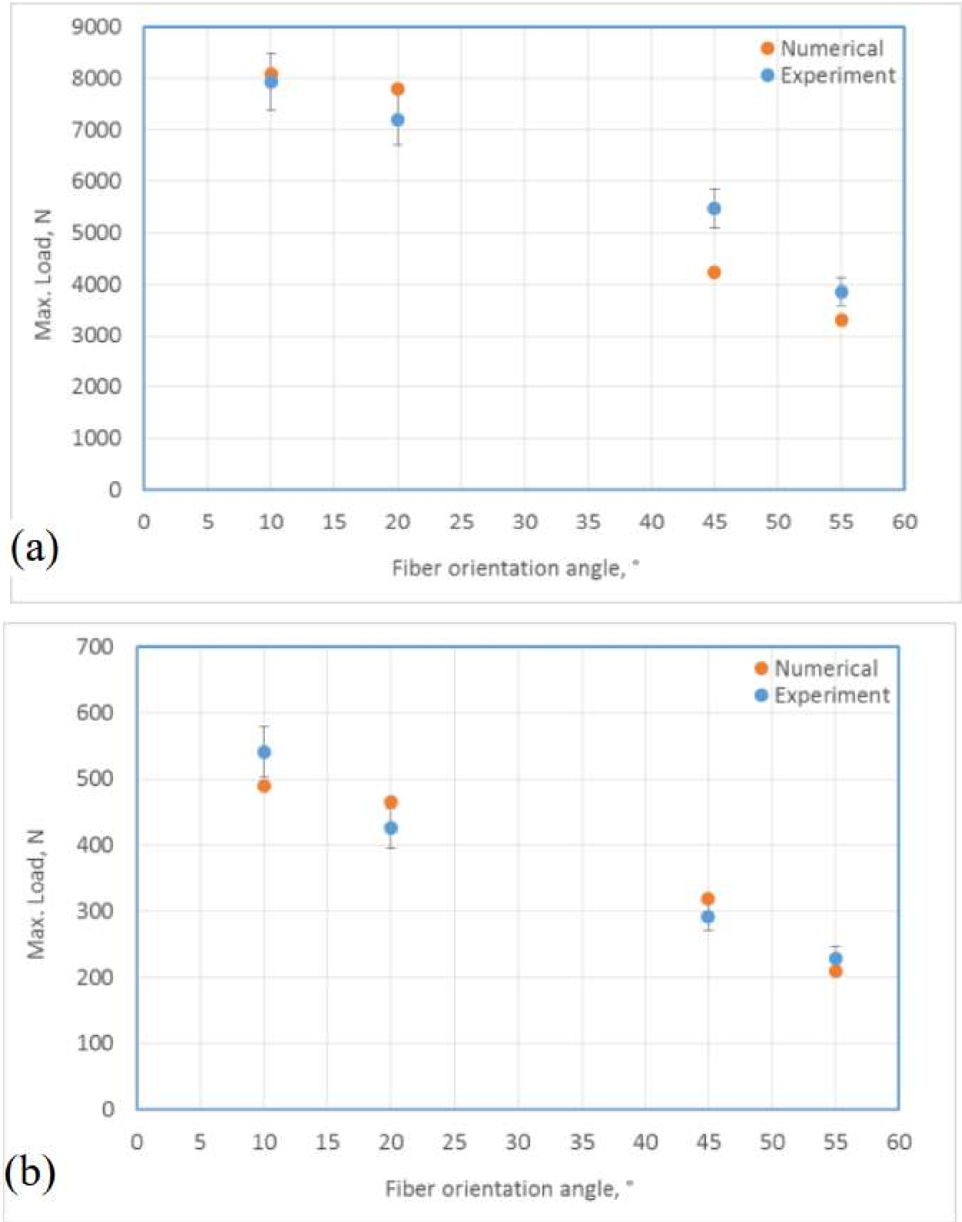

Figure 4.3 Maximum loads obtained from experiments and simulations for different orientations of composite adherends for tensile (a) and bending (b) loading

In this numerical job, Hashin failure criteria were accepted for composite elements failure. In this model, both longitudinal and transverse stresses/strains in tension and in compression were acceptable as failure modes (see Table 4.2).

Table 4.2 Hashin failure criteria [36]

Failure Mode	Condition	Failure criterion
Tensile fiber	$\sigma_1 \geq 0$	$f_1 = (\frac{\sigma_1}{\sigma_{1T}^u})^2 + (\frac{\sigma_{12}}{\sigma_{12}^u})^2$
Compressive fiber	$\sigma_1 < 0$	$f_2 = (\frac{\sigma_1}{\sigma_{1C}^u})^2$
Tensile matrix	$(\sigma_2 + \sigma_3) \geq 0$	$f_3 = (\frac{\sigma_2}{\sigma_{2T}^u})^2 + (\frac{\sigma_{12}}{\sigma_{12}^u})^2$
Compressive matrix	$(\sigma_2 + \sigma_3) < 0$	$f_4 = (\frac{\sigma_2}{2\sigma_{23}^u})^2 + [(\frac{\sigma_{2C}^u}{2\sigma_{23}^u})^2 - 1]\frac{\sigma_2}{\sigma_{2C}^u} + (\frac{\sigma_{12}}{\sigma_{12}^u})^2$

Failure indicators f1, f2, f3, f4 represent each of the four failure modes considered in ply material damage model. When the value of each indicator reaches, damage starts to occur in the respective mode. Damage evolution were modelled by a linear softening response originally proposed for cohesive elements in [28], where equivalent displacement equivalent stress and the fracture energies, G_{ft}, G_{fc}, G_{mt} and G_{mc} energies dissipated during damage of fiber tension, fiber compression, matrix tension and matrix compression failure modes, respectively - were used in the computations. Elastic properties, strength and damage values used in the simulations for the composite plies are given in Table 4.2.

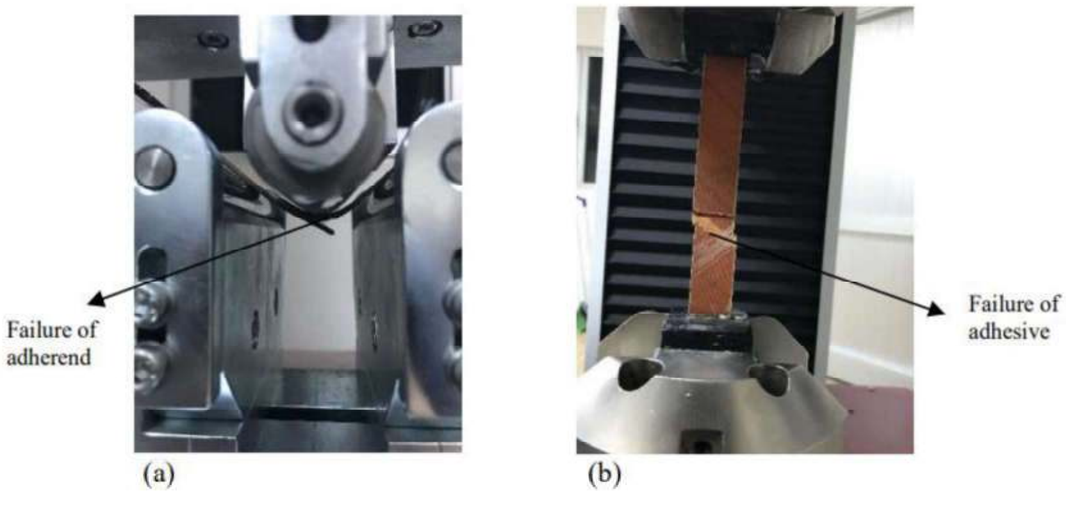

Figure 4.4 Failure mechanisms in the joints under tensile (a) and bending (b) loading for the adherend with 55° ply angle and 25 mm overlap length

Initial results showed that failure mechanisms of the joints is totally different from each other depending on loading modes; while mostly the failure occurred in the adherends for the joints under tensile loading, that mainly took place in the adhesive layer for the joints under the bending loading. In Fig. 4.4, the failure regions are shown for the both loading cases, respectively.

In order to have an in-depth idea, it was investigated that performance of the adhesive under maximum tensile loading for different overlap lengths, the distributions of von Mises, σ_{11}, σ_{22}, σ_{33}, and σ_{13} along line A B in the adhesive layer (Fig 4.5). Here, σ_{11}, σ_{22} and σ_{33} are normal stresses in x, y and z directions, respectively, and σ_{13} is the shear stress in x-z plane. It was observed that not only the pure shear, σ_{13}, ruled the deformation on the adhesive layer, yet there existed a considerable amount of σ_{11} due to bending effect in the region of the overlap. Peel stresses, σ_{33} was also one of the main sources of the concentrations at both ends of the adhesive layer. As the stresses are larger at the edges of the adhesive compared to its mid-region, failure starts from the edges. In general, uniform stresses on the mid-part of the overlap are seen; while the von-Mises stress values are around 20 MPa on this region for the 15 mm overlap length, they are 15 MPa and 12 MPa for the 25 mm and 40 mm lengths, respectively. This can be explained by the fact that since more material volume carry the load when the bonding length increased, stress values dropped.

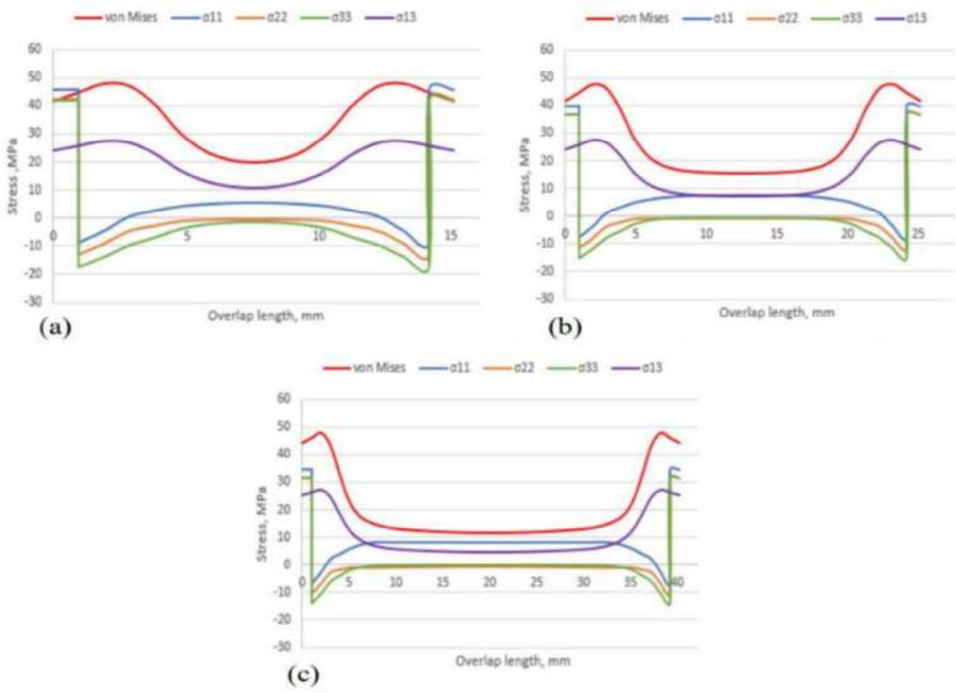

Figure 4.5 The stress distributions along the adhesive layers under tensile loading.

It is also investigated von Mises, σ_{11}, σ_{22}, σ_{33}, and σ_{13} distributions along line C-D (shown in Fig. 4.2(a)) in the adherend when the maximum load was reached. (Fig.4.6). As expected, tensile stress σ_{11} is observed to be the main stress component ruling the deformation. Interestingly, 400 MPa stress value was obtained at the point where the overlapping of adhesive and adherend ended regardless of its length. While this σ_{11} saturate to 200 MPa when overlap length is 15 mm, they are saturated to 280 MPa and 300 MPa when overlap lengths are 25 mm and 40 mm, respectively. We here conclude that increasing the overlap length leads to a more uniform stress distribution on the adherend-excluding overlapping and another edge regions.

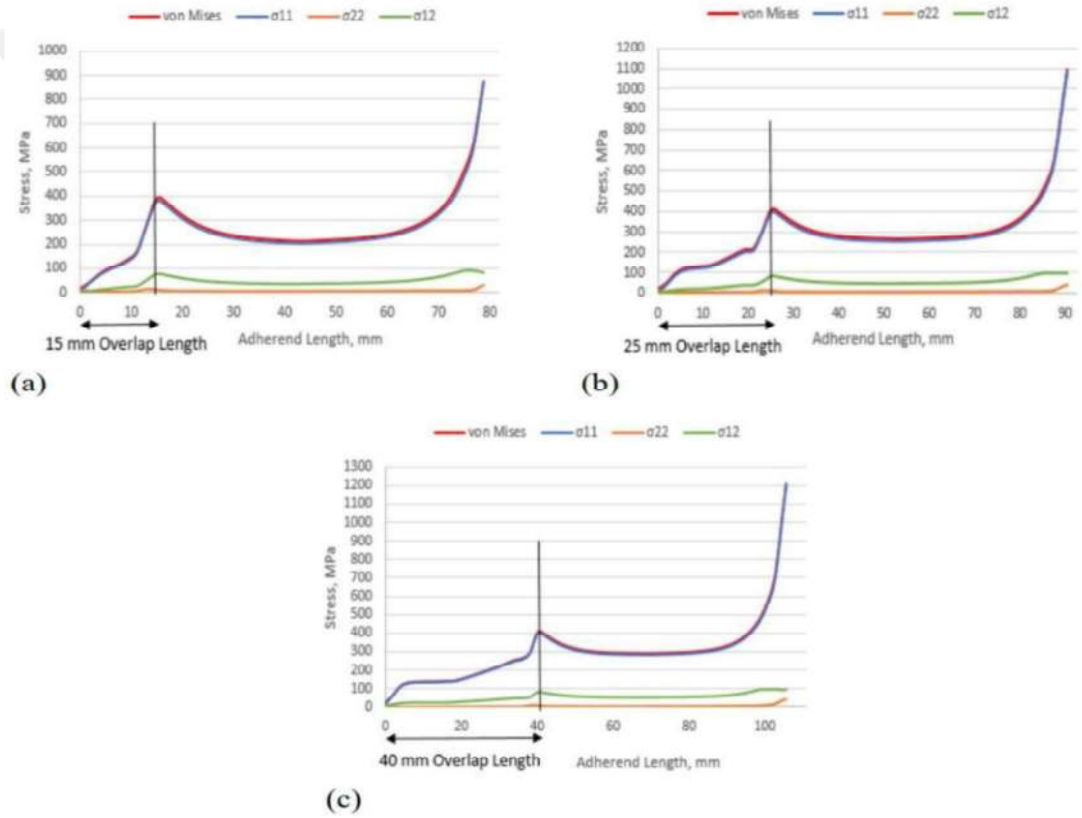

Figure 4.6 The stress distributions along the adherends under tensile loading.

Simulation result of the model for the joint under three-point bending loading is shown in Fig. 4.6(b), which indicates that while one end of the overlap is in tension - as a result of positive σ_{11}, the other end is in compression. This can be also detected from Fig. 4.6, where the distributions of von Mises, σ_{11}, σ_{22}, σ_{33}, and σ_{13} along line E-F (shown in Fig. 4.2(b)) in the adhesive layer for different binding length - when the maximum load was reached - were plotted. This is valid also for the value of σ_{33}, where zone close to the top adhenerd is in tension, the other near the bottom adherend is in compression. Since polymers, so adhesives, in general, are much stronger under compression rather than in tension, one may expect failure starts from the tension side. In line with this prediction, it was experienced experimentally that all initial failures in the joints under bending loading started at the tension side, leading to a complete failure in the adhesive layer (see Fig. 4.4(b)). Similar to the observation in tensile loading mode, a more uniform stress distributions was observed when the overlapping length was increased when Fig. 4.7 was carefully analyzed.

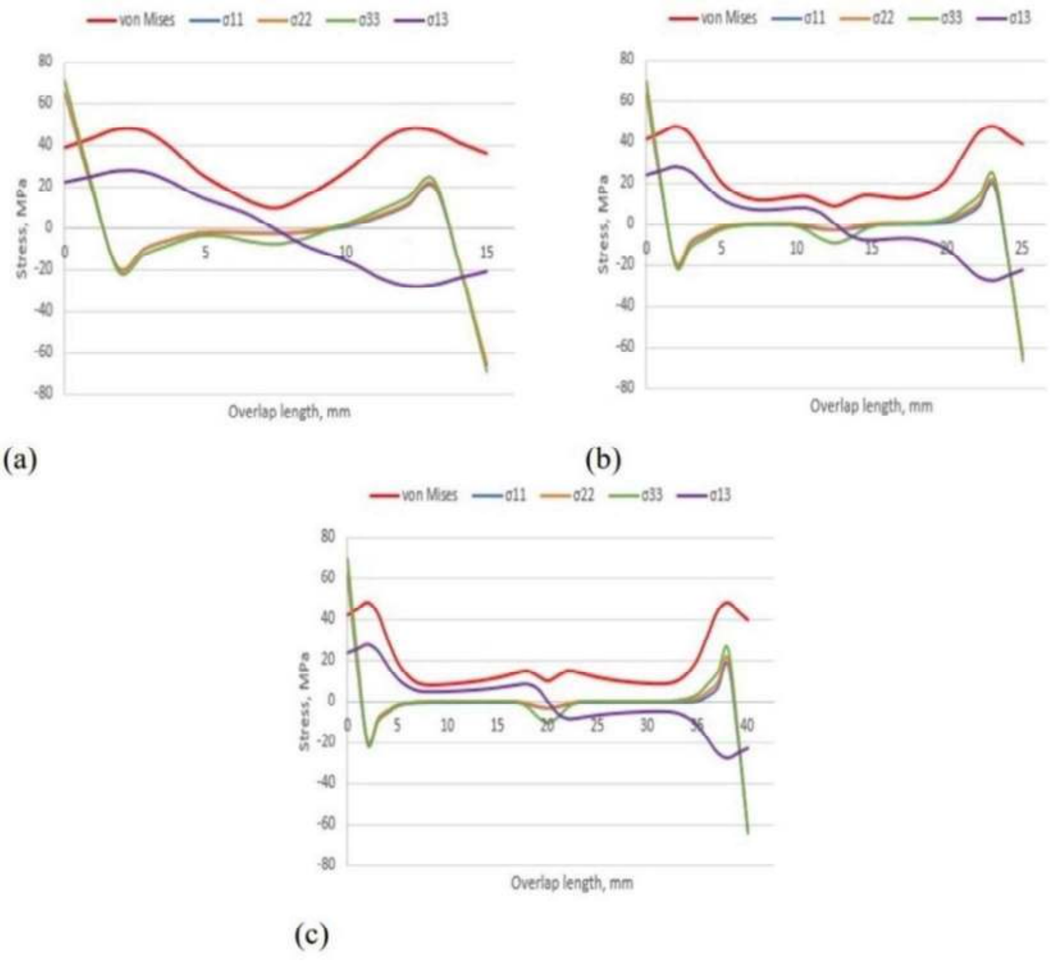

Figure 4.7 The stress distributions along the adhesive layers under three-point bending loading

Simulation result of the model for the joint under three-point bending loading is shown in Fig. 3(b), which indicates that while one end of the overlap is in tension - as a result of positive σ11, the other end is in compression. This can be also detected from Fig. 4.6, where the distributions of von Mises, σ11, σ22, σ33, and σ13 along line E-F (shown in Fig. 4.2(b)) in the adhesive layer for different binding length - when the maximum load was reached - were plotted. This is valid also for the value of σ33, where zone close to the top adhenerd is in tension, the other near the bottom adherend is in compression. Since polymers, so adhesives, in general, are much stronger under compression rather than in tension, one may expect failure starts from the tension side. In line with this prediction, it was experienced experimentally that all initial failures in the joints under bending loading started at the tension side, leading to a complete failure in the adhesive layer (see Fig. 4.2(b)). Similar to the observation in tensile loading mode, a more uniform stress distributions was observed when the overlapping length was increased when Fig. 4.6 was carefully analyzed.

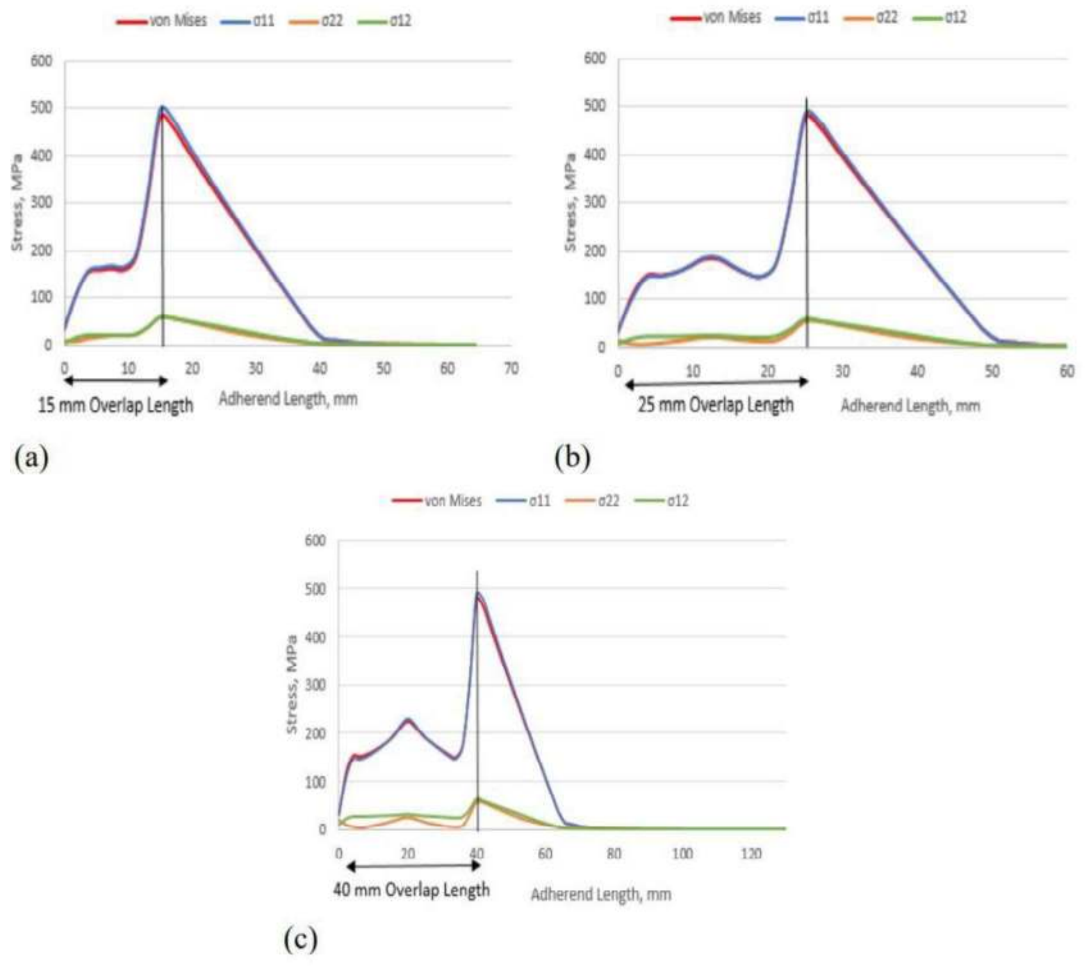

Figure 4.8 The stress distributions along the adherends under tensile loading.

It is also plotted stress distributions along line G-H (shown in Fig. 4.2(b)) in the adherend when the maximum load was reached (Fig. 4.8). Similar to the tensile loading case, peak values are obtained at the points close to the overlap end, which implies either the composite adherend or the adhesive itself could fail at that point because of the stress concentrations. It was also observed that in the course of deformation σ_{11} became the most effective stress in the adherend.

4.2 Investigation of Adhesively Bonded Carbon Fiber Composites

In this part of the study, composite adherents were bonded as shown in the standard [41] and tested in order to determine and observe the damage mechanics in composite materials experimentally. This study was supported by the Turkish Aerospace Industry and the work done within the scope of the study was published in the "Journal of Materials Science and Engineering".[42]

4.2.1 Aim of The Study

In this part, it was aimed to understand the shear performance of adhesives in SLJ configuration in tensile loading and peel effects on the joints with GF composite adherends, however, the adhesive is subject to tensile and bending loads throughout the working life of the joints.[42] For this reason, it was requested to examine these two loading modes. The aim of this study was to investigate the bonding performance of SLJ fabricated with a woven carbon fiber reinforced polymer matrix prepreg and a structural adhesive film. Connections in a single lap configuration are subjected to tensile loading for shear performances and four point bending tests for bending performances.

4.2.2 Materials Used

Single lap joints were produced with AF163-2K(TM), a structural adhesive film made by 3M, and Hexly 8552S/A280-5H, a pre-impregnated version of a woven carbon fiber reinforced epoxy matrix composite made by Hexcel. Mechanical properties of the adhesive was shown before in table *1*. The bonded material is shown in Table 4.3.

Table 4.3 Mechanical Properties of Carbon Fiber

	Materials	σ_{11} (MPa)	σ_{22} (MPa)	E_{11} (MPa)	E_{22} (MPa)
Adherends	Hexply 8552S/A280-5H	850	850	65000	65000

Here, subindexes 11 and 22 represent the coordinate axes in the x and y directions, respectively.

4.2.3 Experimental Works

In this study, care was taken not to affect the test results by keeping the thickness of the adhesive layer constant as 0.2mm. Two different adherend thicknesses of 2 mm and 3 mm and three different overlap lengths of 15 mm, 25 mm and 40 mm were used for the parametric study.

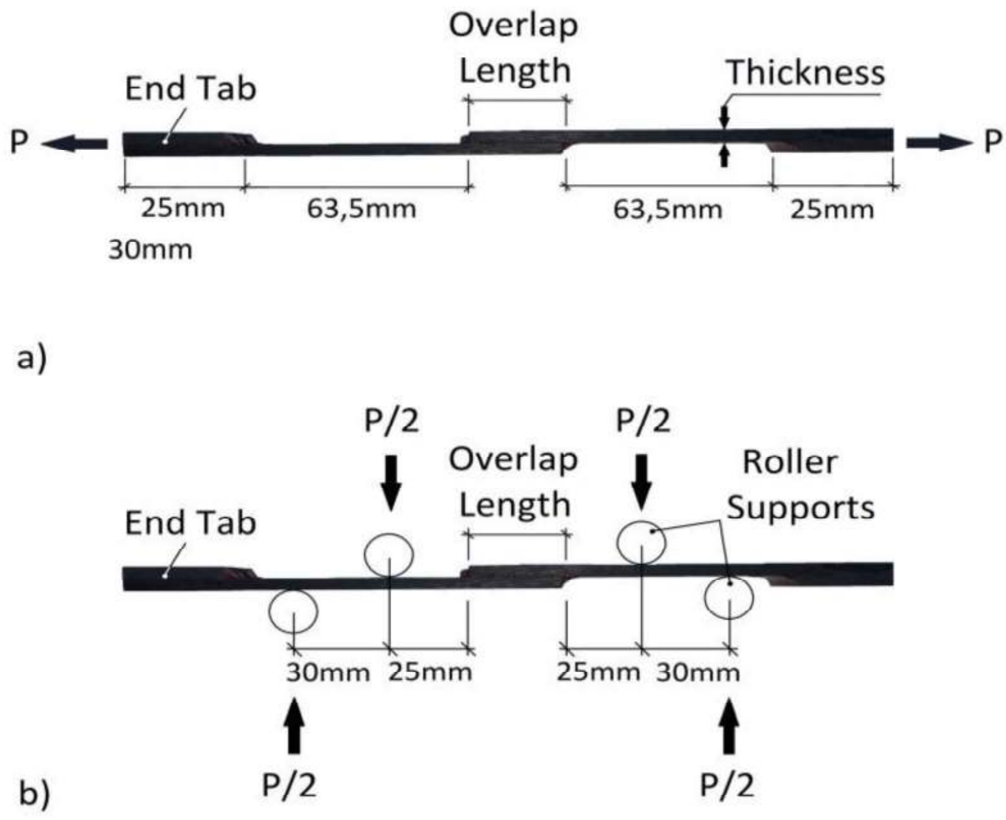

Figure 4.9 Dimensions of the SLJ configuration in a) tensile and b) bending loading

The adhesive used was cured at 125 °C for 60 minutes under a pressure of 2 bar, while the curing procedure for pre-impregnation of composite adhesives was 120 °C for 120 minutes after an initial heating procedure of 80 °C. 90 minutes at 5 bar pressure. Adhesives were produced from the plates of cured prepregs and machined to the required dimensions. The joints were bonded in a specially designed mold that allowed samples to be produced with different bond thicknesses and different overlap lengths.

4.2.4 Results

The geometric details of the tested single lap joint (SLJ) specimens, prepared according to the dimensions specified in the ASTM D-1002 standard, are shown in Figure 4.9. The surface preparation of the adhesives to be bonded was made by peeling method as the only surface preparation technique and all samples were tested at 23 ^{0}C room temperature and 50% relative humidity in order to avoid the effects of different environmental conditions. Four samples for each type were tested to see if the results were reproducible. Some mechanical properties of the bonded material and adhesive film are shown in Table 4.1, where σ and E and υ; tensile strength value, Young's modulus and Poison ratio of the materials used. Here, subindexes 11 and 22 represent the coordinate axes in the x and y directions, respectively.

The load curves corresponding to the crosshead displacement of joints with bond thicknesses of 2 mm and 3 mm, respectively, for different overlap lengths under tensile load are shown in Figures 4.10a and 4.10b.

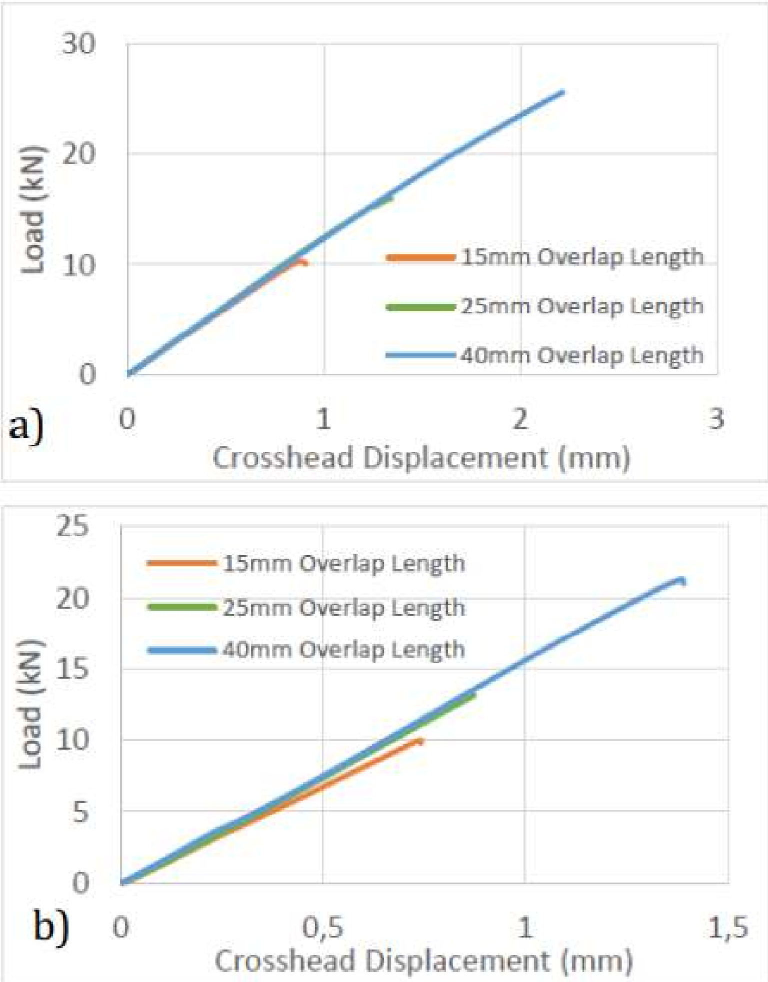

Figure 4.10 Overlap lengths under tensile loading a)2mm adherend b)3mm adherend.

The curves show that increasing overlap lengths leads to an increase in displacements, which is indicative of the high energy stored in the samples. Fracture load versus overlap length is shown in Figure 4.11a for both bonded thicknesses. The figure shows that there is a generally linear relationship between the breaking load and the overlap length, and the effect of different carbon fiber bonding thicknesses on the breaking load is not significant.

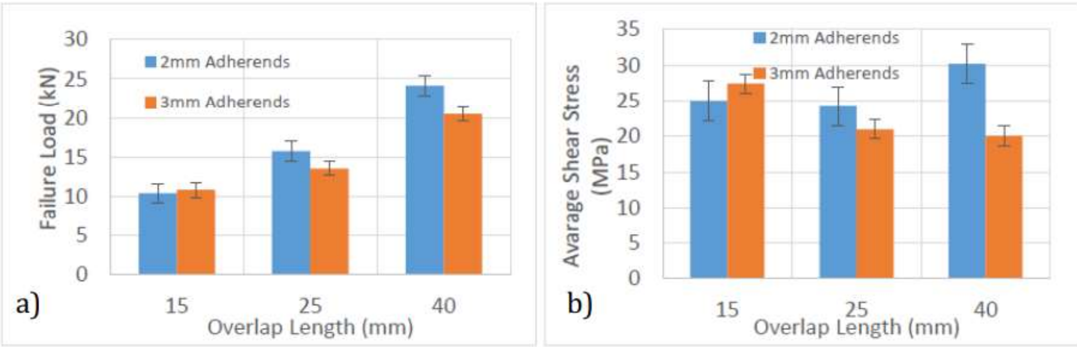

Figure 4.11 a) Failure load against overlap length and, b) Average shear stress against overlap length for the SLJ in tensile loading

Samples with 3 mm adherend thickness and 40 mm overlap length less fracture load than samples with 2 mm thickness with the same overlap length. While the minimum breaking load is approximately 10 kN in 15 mm overlap length connections, the maximum value is approximately 24 kN in 40 mm overlap length connections, and the fracture load is approximately 15 kN in 25 mm overlap length. A plot of mean shear stress versus overlap length is presented in Figure 3.11b. Joints with adhesion thickness of 2 mm and 3 mm showed tensile values of 20 MPa and 30 MPa, respectively. It is seen that the joints with 2 mm bonding thickness generally show higher shear stress values than the 3 mm connections, which is thought to be due to the large load eccentricity in thicker bondings.

For the tensile-shear test, all specimens with overlapping lengths of 15 mm and 25 mm showed breakage in the adhesive layer (Figure 4.12a) under breaking loads. Those with overlay lengths of 40 mm experienced damage to the adhesive layer itself as well as damage to the composite layers adjacent to the adhesive layer (Figure 4.12b).

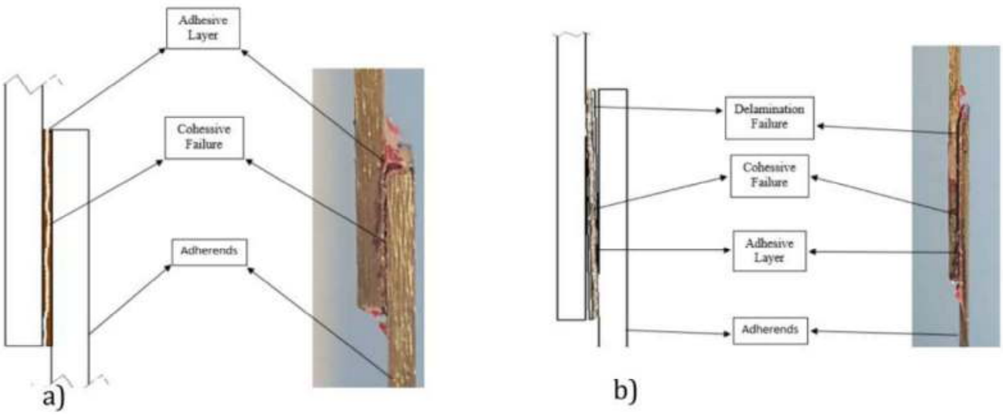

Figure 4.12 Load against crosshead displacement for the SLJ specimens in bending loading, for the adherends with a) 2 mm and b) 3 mm thicknesses

In this case, more damage occurred to the composite plies at the 3mm joints compared to the 2mm joints. It was evident that higher adherend thickness joints experienced greater peeling effects at the ends of the overlap length due to eccentrically applied loading, which could be the cause of more ply damage. Stress concentrations at the end of the overlap (peeling effects), stress distributions in the adhesive layer in the SLJ configuration were investigated in the numerical study shown in chapter 4.1 for glass fiber joint in this study. It was seen that stress distributions were not uniform. As in the sample shown in figure 4.13a, adhesive layer fracture occurred in all joints with 15 mm and 25 mm overlap lengths. In this case, no initial breakage was observed in the bonded parts. As a result, it can be interpreted that the fracture mechanism that occurs in response to the loading is approximately symmetrical. Stress concentrations from peeling effects were seen at the ends of the link. For joints with a lap length of 40 mm, interfacial rupture was found to occur not only on the adhesive, but also on the composite layers adjacent to the adhesive layer (Fig. 4.13b).

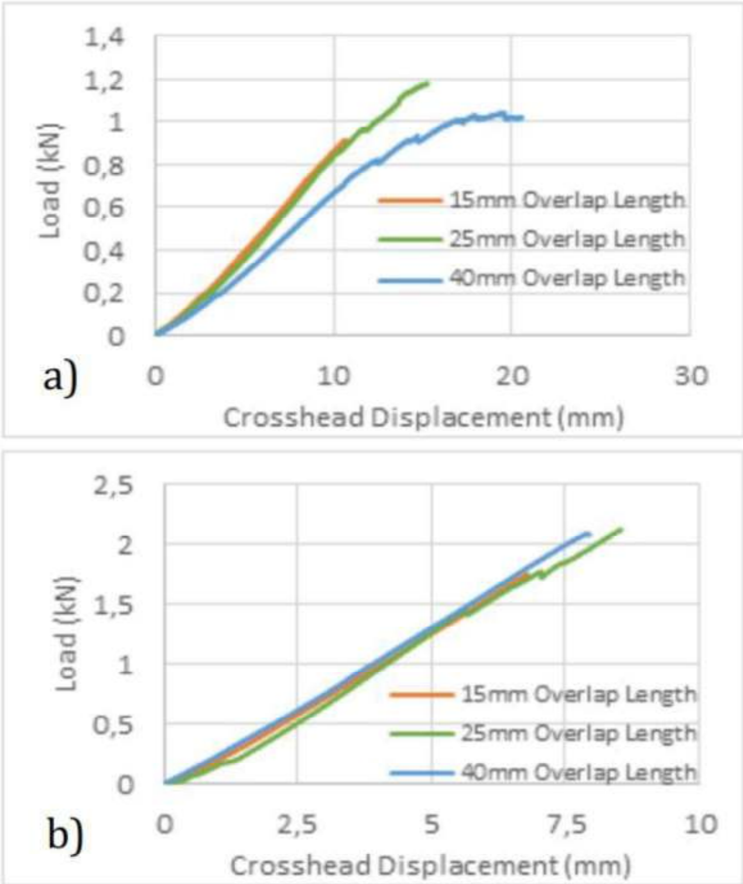

Figure 4.13 Plots of load against crosshead displacement for the SLJ specimens in bending loading, for the adherends with a) 2 mm and b) 3 mm thicknesses

Crosshead displacement for joints with 2 mm and 3 mm adherend thicknesses are shown in Figures 4.13a and 4.13b, respectively. From the curves, increasing lap length did not cause an important increase in fracture load and crosshead displacement; All joints with 2 mm adherend thickness deteriorate around 1000 N, and at 3 mm joints around 2000 N. Since the adherend, which bends with less deflection, bends in a more rigid form, it is thought that when it is subjected to bending, it creates a softer stress distributions at the end points over the bonding region than the thin one.

For all lap lengths and adherend thicknesses under flexural loading, adhesive failure was not observed and Composite ply adjacent to the adhesive layer damage was observed. During the test no failure was observed in the adhesive layer. As seen in Figure 4.13b, one end of the overlap region is in tension (right side) and the other end is in compression (left side), which are the points where damage is expected to begin. As seen in the previous study, these stresses also cause high stress peaks on the adherend. For this reason, it is an expected result that the stresses caused by bending cause delamination damage by removing the layer from the composite material.

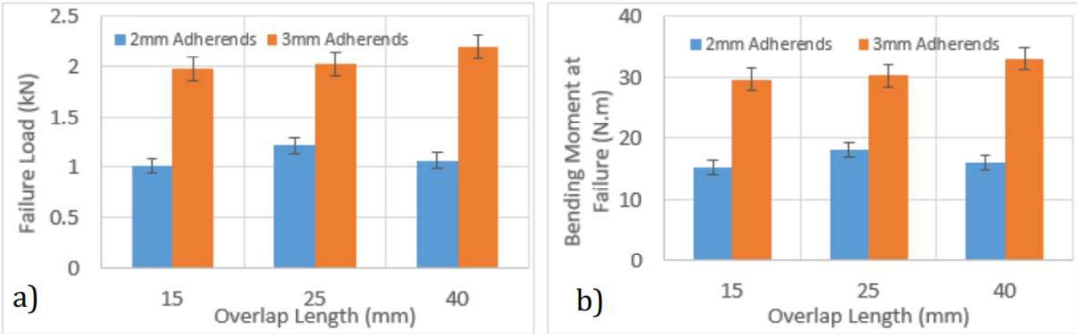

Figure 4.14 a) Failure load against overlap length and, **b)** Bending moment against overlap length for the SLJ in bending loading.

Some representative curves of bending load against crosshead displacement for the joints with 2 mm and 3 mm adherend thicknesses are shown in Figs. 4.13a and 4.13b, respectively. From the curves, it is seen that increasing overlap length does not result in a significance increase in the failure load and crosshead displacement; while all the joints with 2 mm adherend thicknesses fail about 1000 N, those with the 3 mm fail around 2000 N, implying an increase of 100% for the thicker adherends. This is considered to be due to the relatively small deflection of the thick adherends experiencing under the bending, compared to the thin ones, which is believed to have important effects on the stress concentrations at the edges of the overlap length, the main cause of failure initiation. Figs. 4.14a and 4.14b show the plot of the bending failure load and the bending moment against the overlap length, respectively, which indicate the values from the thick adherends double compared to the thin ones, which is again related to the adherend deflections under the bending.

4.3 Dynamic Behavior of Single Strap Joints (SSJ)

During the preparation of this thesis, in the next part of the study, while performing high speed ballistic tests on the samples, vibrations occur that cause significant effects on the material behavior. In order to obtain information about the vibration behavior of composite joints, it was deemed appropriate to conduct a series of experimental studies.

In this part of the study, the dynamic behavior of glass fiber reinforced composite adherends and straps and SSJs were measured and interpreted using the vibrating beam technique. The effects of the straps with different stacking sequences of ±450 angles on the dynamic performance of the joints were investigated. Special attention has been paid to damping ratios for SSJs.

The findings from the studies in this section were published at the Sampe nexus 2021 conference and the study was supported by the Turkish Aerospace Industry.

4.3.1 The Aim of The Study

The study aims to test SSJ's with clamped-free end conditions to find natural frequency of the samples using vibrating beam tecnique. Numerical modal analysis of joints was also performed to find out and compare their natural frequencies and mode shapes.

4.3.2 Materials Used

The Adherends and straps used in this study were manufactured from Hexly913/33/UD280 prepreg material produced by Hexcel and cured in an autoclave at the temperature range of 120-180 ^{0}C, under 5 bar pressure approximately, with heating rates of 0.5-3.5 ^{0}C/min [44]. All the adherends were prepared with only unidirectional (0^0) oriented ten plies. Adherend longitudinal dimensions were prepared in 101 and 111 mm lengths to be used depending on the strap length. Straps produced with four different orientation angle with ten layers and two different lengths (25 mm and 45 mm) were used. The final dimensions of the specimens presented in Table 4.4.

Table 4.4 Specimen measurements

Length of Adherends (mm)	Length of Straps (mm)	Equiv. thickness of the SSJ (mm)	Width of the SSJ (mm)	Mass of the SSJ (gr)	Equiv. Density of the SSJ (kg/m^3)
101	25	2.81	25	23.91	1794.95
111	45	2.81	25	28.00	1794.95

Three types of configurations were produced with eight layers 0^0 fiber angle and $\pm45^0$ angle two layers placed on top, bottom and in the middle of layers, and the last one was ten layers 0^0 angle configuration. After all, the specimens were put in an autoclave to cure the adhesive layer and to get the bonded joints, which were subjected to a temperature of 120^0C and 3 bars of pressure for 90 minutes [45]. The final configurations of the specimens presented in figure 4.15 illustrates; S1- the one with totally ten 0° angle plies, S2- the one with eight plies of 0° and two plies of 45° located in the middle of the strap (-450 in the fifth and $+45^0$ sixth layer), S3- the one with eight plies of 0° and two plies of 45° located on the outer surface of the strap (-45^0 in the ninth and +45 tenth layer), and S4- the one with eight plies of 0° and two plies of 45° located in the inner surface of the strap close to the adhesive layer (-45^0 in the first and $+45^0$ second layer).

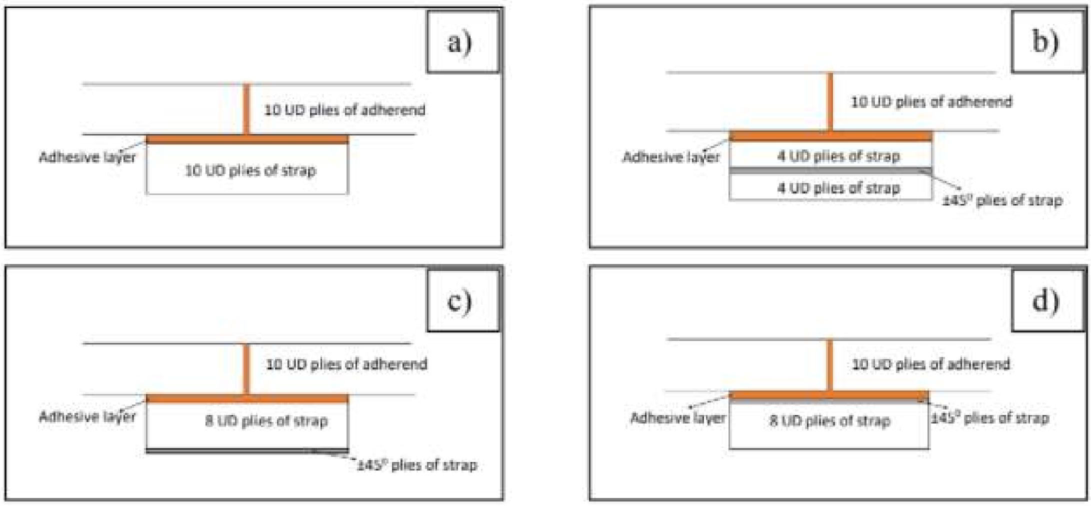

Figure 4.15 The specimens with different types of straps; a) S1, b) S2, c) S3,and d) S4

4.3.3 Experimental Study

The samples were tested as shown in the figure by generating vibration with an instrumented impact hammer (8206 Bruel & Kjaer) and receiving the response with a non-contact microphone (Type 1706/8206 Bruel & Kjaer) in a vibrating beam test setup. It is aimed to display the natural frequencies of the samples affected by the hammer, depending on their mode shape, through high amplitude peak values in a certain frequency range. In order to collect the digital answers from the microphone, the advanced data acquisition card HBM QuantumX MX410B, which can collect data up to 200K per second, was used by connecting to the computer. The natural frequency, bending stiffness and damping values of the samples were measured with this test set-up as seen in the figure 4.16.

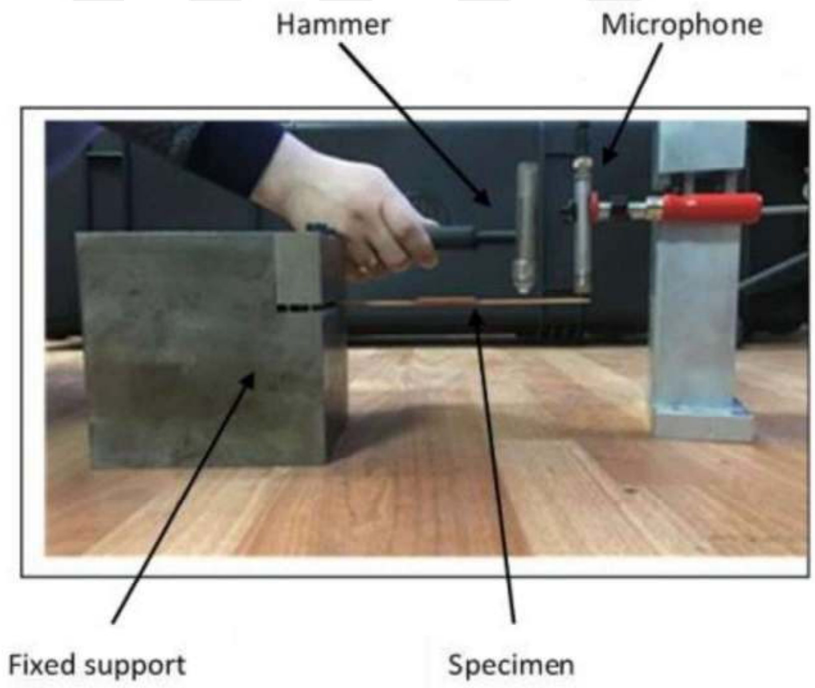

Figure 4.16 The experimental test set-up for modal analysis.

For the damping values, the half power bandwidth method [43] was used. It is important to note that the specimens were placed into the fixed support properly and the clamped part was tightened firmly, which was crucial for reliable measurements. For each category of the specimens, two different specimens were tested to see if repeatable experimental results were obtained, and average results with percentage deviation were presented.

4.3.4 Numerical Study

A numerical modal analysis model of the SSJs with fixed-free boundary conditions was conducted using the finite element analysis through ABAQUS package program. A three dimensional (3-D) meshed model of the joint is presented in the Figure 4.17.

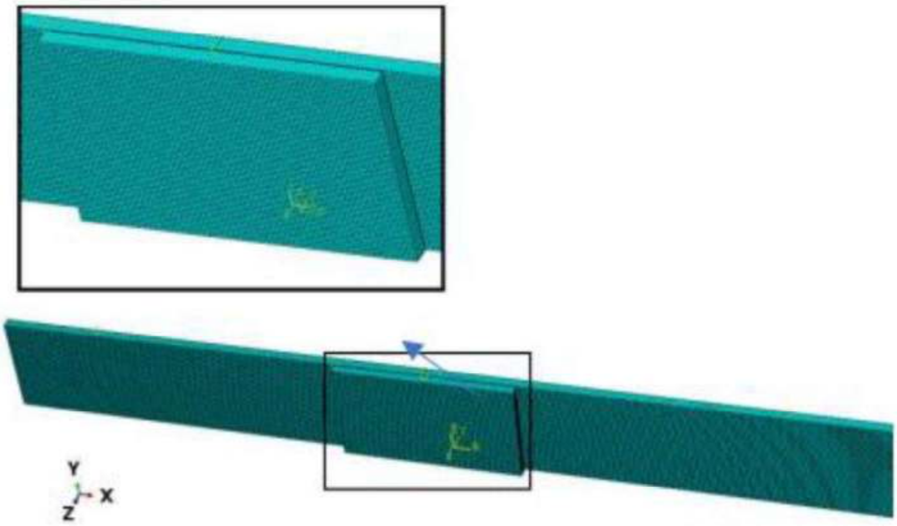

Figure 4.17 Single Strap Joint (SSJ) 3D meshed numerical model.

The element type used for the adhesive layer was C3D8R that is an 8-node linear brick, reduced integration with hourglass control. For the adherends and straps the element type used was SC8R that is an 8-node quadrilateral in-plane general purpose continuum shell, reduced integration with hourglass control, finite membrane strains. Natural frequencies, mode shapes and flexural rigidity of the joints were predicted and compared with the experimental results. Note that only the first mod frequency was used for to compare the reasons.

Table 4.5 Input data used for the modal analysis

Materials	E_1 (MPa)	E_2=E_3 (MPa)	G_{12}= G_{13} (MPa)	G_{23} (MPa)	υ_{12}= υ_{12}= υ_{23}	ρ (kg/m^3)
Laminate Hexply 913/33%	44000	13000	6900	6300	0.27	1800
Adhesive Film (AF163-2K)	2000	-	-	-	0.34	1100

For the preparation of numerical analysis, the required material property input datas are shown in Table 4.5.

4.3.5 Results

The experimental values of the fundamental natural frequency, the equivalent flexural rigidity and the specific damping capacity (SDC) of the specimens are presented in Table 4.6.

Table 4.6 A comparison of experimental (Exp.) and predicted (Pred.) results.

Specimens	Strap Length (mm)	Exp. NF* f_n (Hz)	Pred. NF* f_n (Hz)	Exp. FR* EI (Pa.m^4)	Pred. FR* EI (Pa.m^4)	Exp. SDC* (%)
S1	25	57.15	60.40	3.20	3.57	3.33
S2	25	56.20	60.38	3.09	3.57	7.39
S3	25	56.32	60.39	3.10	3.57	8.12
S4	25	55.88	60.35	3.06	3.56	7.63
S1	45	47.22	49.30	2.18	2.38	3.25
S2	45	46.94	49.27	2.16	2.38	8.26
S3	45	47.11	49.29	2.17	2.38	7.88
S4	45	46.81	49.23	2.14	2.37	8.21

* NF: Natural Frequency, FR: Flexural Rigidity, SDC: Specific Damping Capacity

The maximum values of the frequency and flexural rigidity are belonging to the joints with 25 mm length of straps with the 0^0 angle (S1), about 57.15 Hz and 3.20 Pa.m^4 , respectively. These values are 47.22 Hz and 2.18 Pa.m4 for those with the 45 mm strap lengths, respectively. The value of the SDC for these specimens is about 3.30%, a minimum, compared to the others (S2, S3 and S4). On the other hand, the specimens with the ±450 angle plies of the straps have relatively lower values of the natural frequency and flexural rigidity, about 56 Hz and 3.10, respectively, but quite considerable higher damping values, 7.39%, 8.12% and 7.63 for the S2, S3 and S4 for the joints with 25 mm strap length, respectively. In this case, the increase in the damping value is about 130%, while the decrease in the value of flexural rigidity is only about 3.43%. It seems the joints with the 45 mm strap length has lower values of the frequency and flexural rigidity but a very small increase in the damping value if compared to those with the 25 mm strap length. The increase in the damping value is about 5.5% but the decrease in the flexural rigidity is about 35% in average.

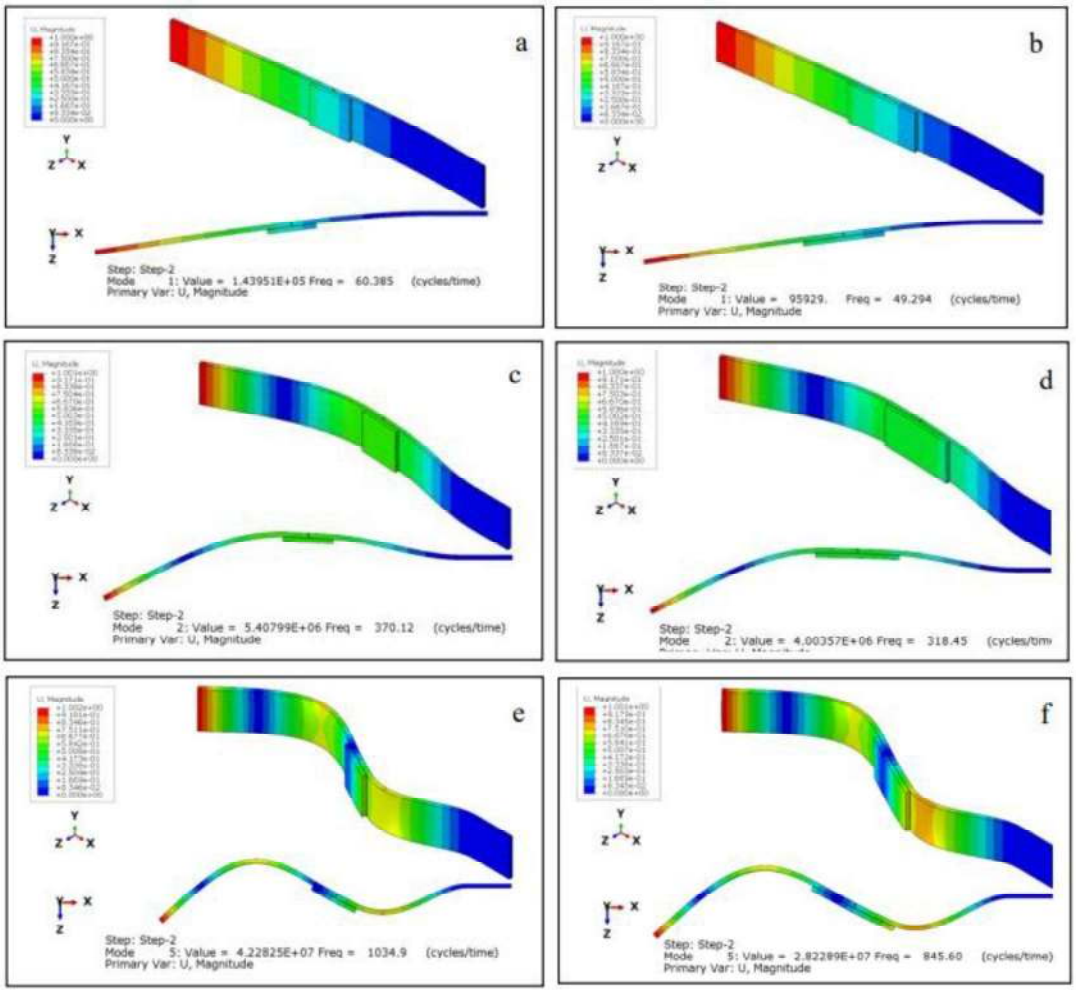

Figure 4.18 a, b) first, c, d) second, and e, f) third mode shapes of the SSJs with 25 mm and 45 mm strap lengths, respectively.

It is believed that the rigidity decrement is due to the relatively longer length of the joints with the 45 mm strap (222 mm), compared to those with the 25 mm strap length (202 mm), while they both have the same amount of thickness. Figure 4.18 indicates the first, second and third mode shapes of the SSJs with their predicted natural frequencies. The figure is a representative predicted shape to the joints with 25 mm and 45 mm strap lengths. Note that only first predicted natural frequencies were used and compared with the experimental ones presented in Table 4.6.

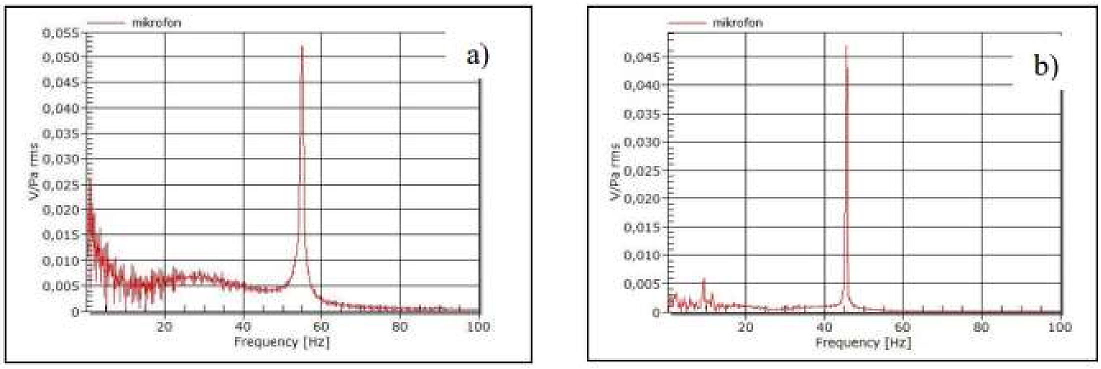

Figure 4.19 Two representative outputs from the vibrating beam test set-up with fixed-free boundary conditions; a) the SSJ with 25 mm strap length, b) the SSJ with 45 mm strap length.

Figure 4.19 shows two representative experimental outputs obtained through the software used. It can be seen clearly peak frequency values from the software interface chart.

This work proves that it is possible to increase the damping performance of adhesively bonded joints by shifting some parameters that do not compromise the flexural rigidity too much. In the case of the SSJs, inclusion of ±450 plies into the strap laminates have enhanced the damping performance considerably. It is worth pointing that structural damping is seen as important parameter for the design of vehicles and machines.

CHAPTER 5

INVESTIGATION OF METAL TO METAL BONDED JOINTS UNDER HIGH LOADING RATES.

5.1 To Prediction Metal to Metal Bonded Joints With Quasi Static Material Conditions

The most commonly used test methods for structural adhesives and/or adhesive joints under high loading rates are pendulums, drop weight impactors and split Hopkinson pressure bars as seen from the literature view. In structural applications, adhesives are preferably loaded in shear mode to gain the best bond performance. In aerospace applications, it cannot be expected that the joints to be under the shear effect, especially under ballistic conditions. In this study, a special shooting range was set up and was shot from approximately the middle point of the metal-metal bonding area, with a laser pointer. Velocity information of the impacted bullet was obtained by using imaging technique with a high-speed camera. Under the boundary conditions of the experimental setup, the test applied to the samples was modeled with the Abaqus package program, and the experimental results were tried to be verified with the numerical analyzes obtained. The prediction was made according to the worst scenario that account the input data obtained from the quasi-static conditions.

Limited portion of this study was presented at the 36th conference of the American society for Composites on composite materials in 2021. [55] The paper of the expanded version of the article was sent for publication in Reno to USA.

5.1.1 Experimental Works

Because of the joints subjected to the impact test was expected to experience both tensile as well as compression normal stresses under the applied dynamic load, to observe the failure loading values of the materials, tensile and compression tests of the adhesive to be used were carried out using a Besmak BMT-S 100 kN universal testing machine to obtain its stress-strain curve.

5.1.1.1 Sample Preperation

The SLJs were manufactured from 6061 aluminyum adherend (AA6061) materials, and an adhesive film (AF163-2K), a knit film made of thermosetting modified epoxy produced by 3M Scotch-Weld™. The surface portion of the adherend to be bonded was cleaned with acetone, and then the adhesive film was applied to the substrate taking care to minimize the amount of air entrapped as a result of application. All the SLJs were manufactured using a specially designed jig in which the specimens were allowed to be manufactured with different adherend thicknesses and different overlap lengths. The jig was put in digitally controlled oven to cure the joints for 60 minutes at a temperature of 125°C with a pressure of around 2 bar as the supplier recommended. The manufatured joints had an overlap length 25 mm, an adherend thickness of 4 mm, and an adhesive layer thickness of 0.2mm.

5.1.2 Experimental Setup

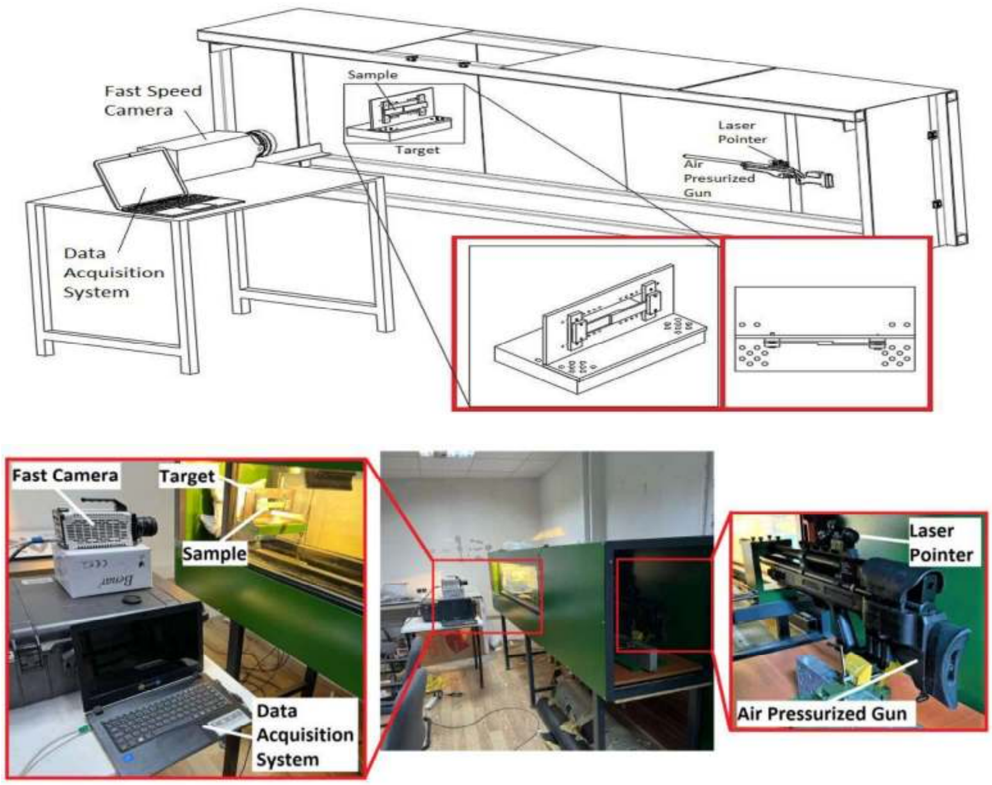

Figure 5.1 The experimental set-up used for the ballistic tests.

The experimental set-up used for the ballistic tests of the joints that composed of a high speed camera, an air-pressurised gun, a data acquisition system, a clamped-clamped fixation for the specimens and a test cabin was shown in Figure 5.1. In this setup, the air rifle was aimed at the desired point on the target from a distance of about 3 meters and the shot was made. The shotted projectile was photographed with the fast camera in order to determine the projectile speed just before it collided. Depending on the frame rate of the camera, the path traveled by the bullet between two consecutive frames recorded by the camera was determined, and the path that the bullet could travel in one second time period was calculated. A real image of the fired bullet with a distance measuring ruler is shown in Figure 5.2.

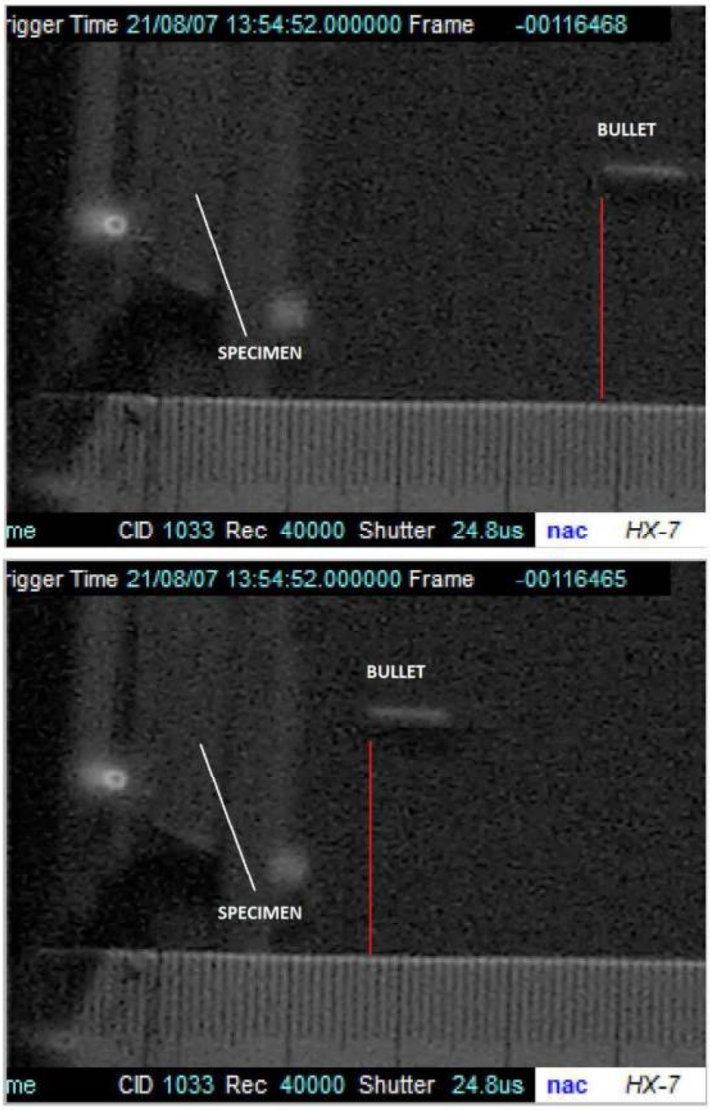

Figure 5.2 A real image of the fired bullet

5.1.3 Numerical Model

For the prediction behavior of the SLJ under the impact loading, a Finite Element Method was used via ABAQUS package program. The specimen was modelled using clamped-clamped boundary conditions. A detail about the dimensions of the specimen and its boundary conditions are shown in Figure 5.3. The C3D8R element type with general purpose linear brick element and reduced integration was used for the analysis. A lead bullet with a weigth of 1.25 gr and density of 11.3 gr/cm^3 was modelled as a projectile. The projectile with the stress-strain curve shown in Figure 4.5 and with 100 m/s velocity were used as input data in the analysis.

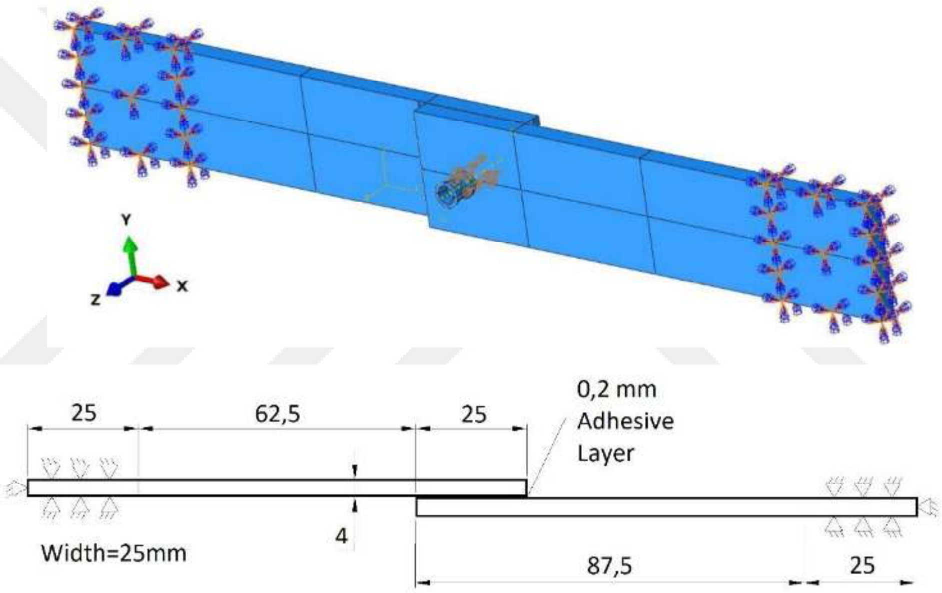

Figure 5.3. The boundary conditions and dimensions of the SLJ used in the numerical analysis

Stress-starin curves of the materials are presented in Figure 5.4 and Figure 5.5, for the adherend and the adhesive, respectively. And also materrial properties for the projectile shown in figure 5.6.

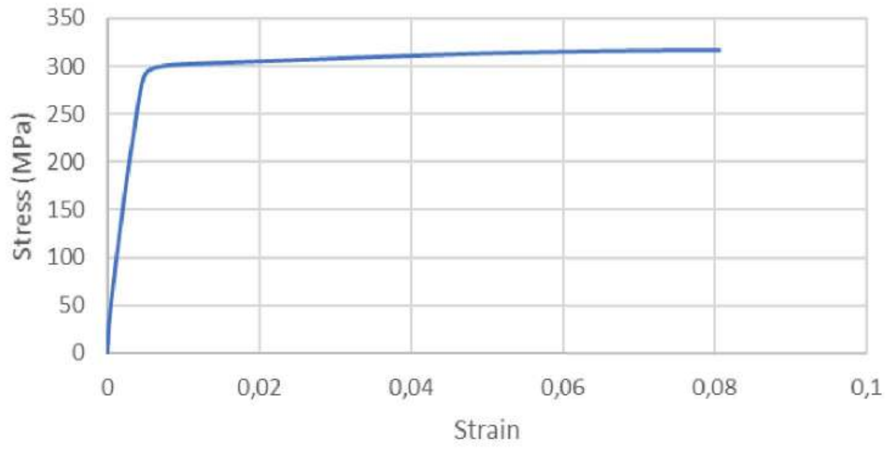

Figure 5.4 Stress-Strain Curve for Al 6061

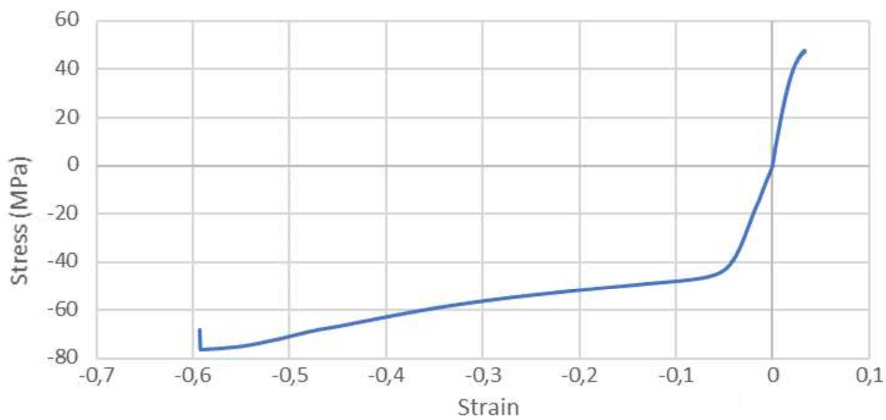

Figure 5.5 Stress-Strain Curve of Af-163-2 Structural Film Adhesive.

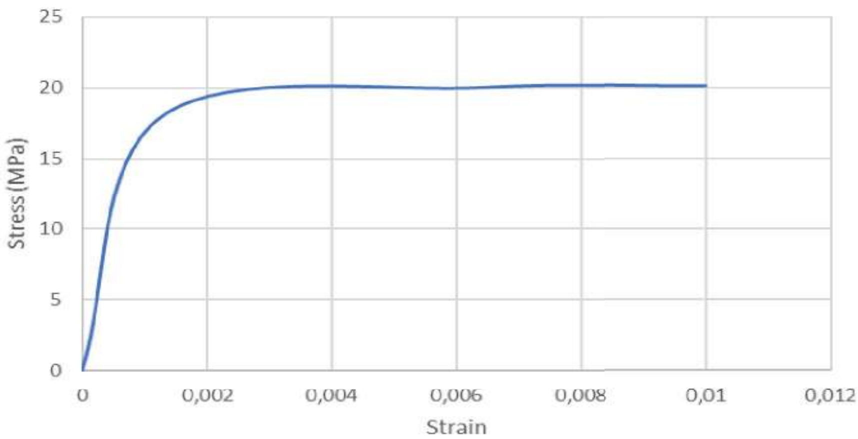

Figure 5.6 Stress-Strain Curve of the projectile used in the numerical analysis.

5.1.4 Results

Figure 5.7 shows curves of predicted velocity-time and also force-time of the impacted adhesive joint. The orange and blue colors represent the variation of velocity and force versus time, respectively.

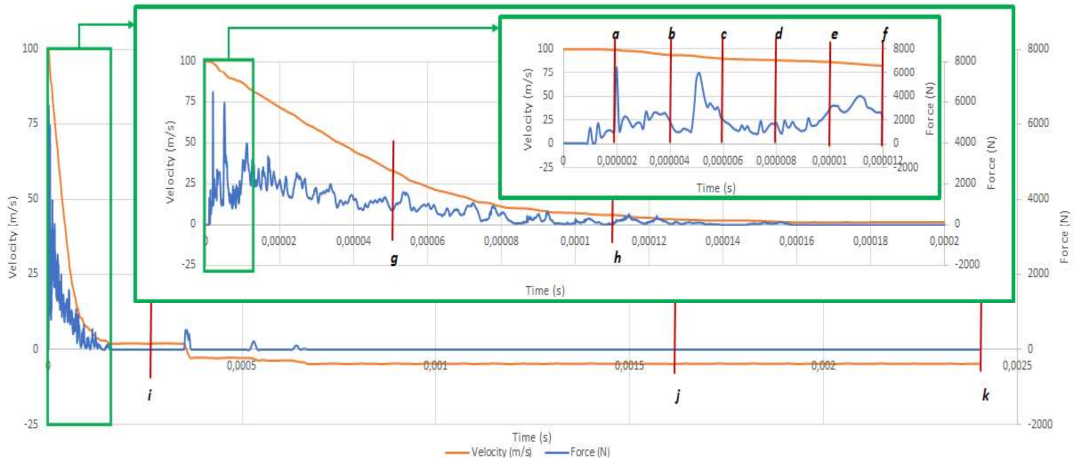

Figure 5.7. The predicted curves of velocity and load with respect to time for the joint under the projectile impact**.**

From the figure, it seems the bullet impacts the joint with a velocity of 100 m/s, and then decays gradually, and finally comes to end at about 0.16 milliseconds (ms). When the velocity is a maximum, the force is zero due to a lag time of reaction. The region where the joint experiences high amount of bending loading has been magnified and labelled as a-b-c-d-e-f. It is seen that the force fluctuates with respect to time after the impact takes place. As the velocity decreases from region g to i, the value of force decreases too, and the bullet starts to move in the opposite direction in the region of j-k, as a result of the strain energy accumulated in the impacted joint. This is confirmed by Figure 5.8 that indicates high levels of von Mises stress of the adherend in the region of a-f, but relatively low stresses beyond this region; the maximum value of von Mises stress in the adherend is about 291 MPa that leads to a local plastic deformation of the adherend that is not expected to cause failure in the adhesive layer.

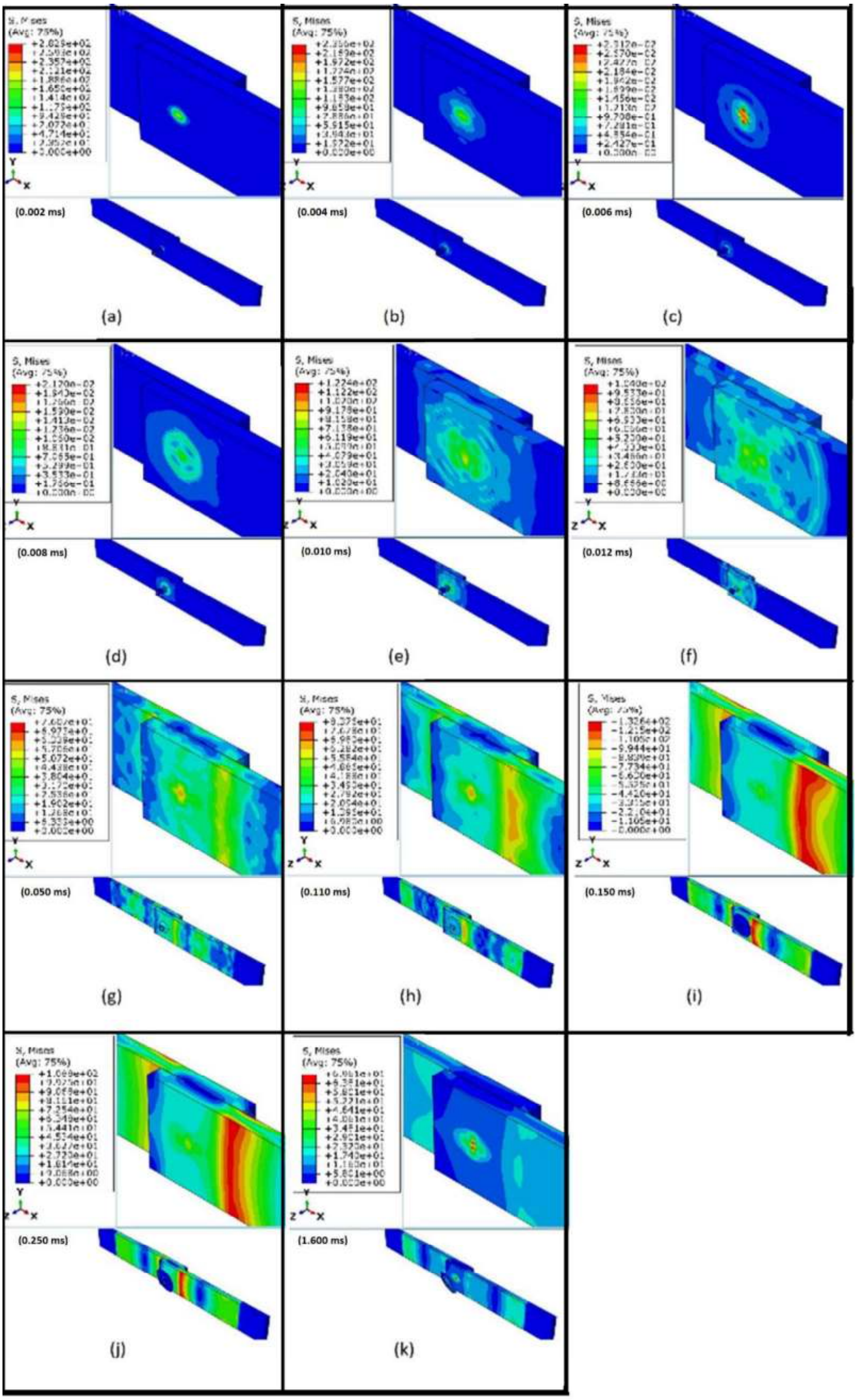

Figure 5.8. The predicted time-dependent von Mises stress (S) of the joint under the impacted loading

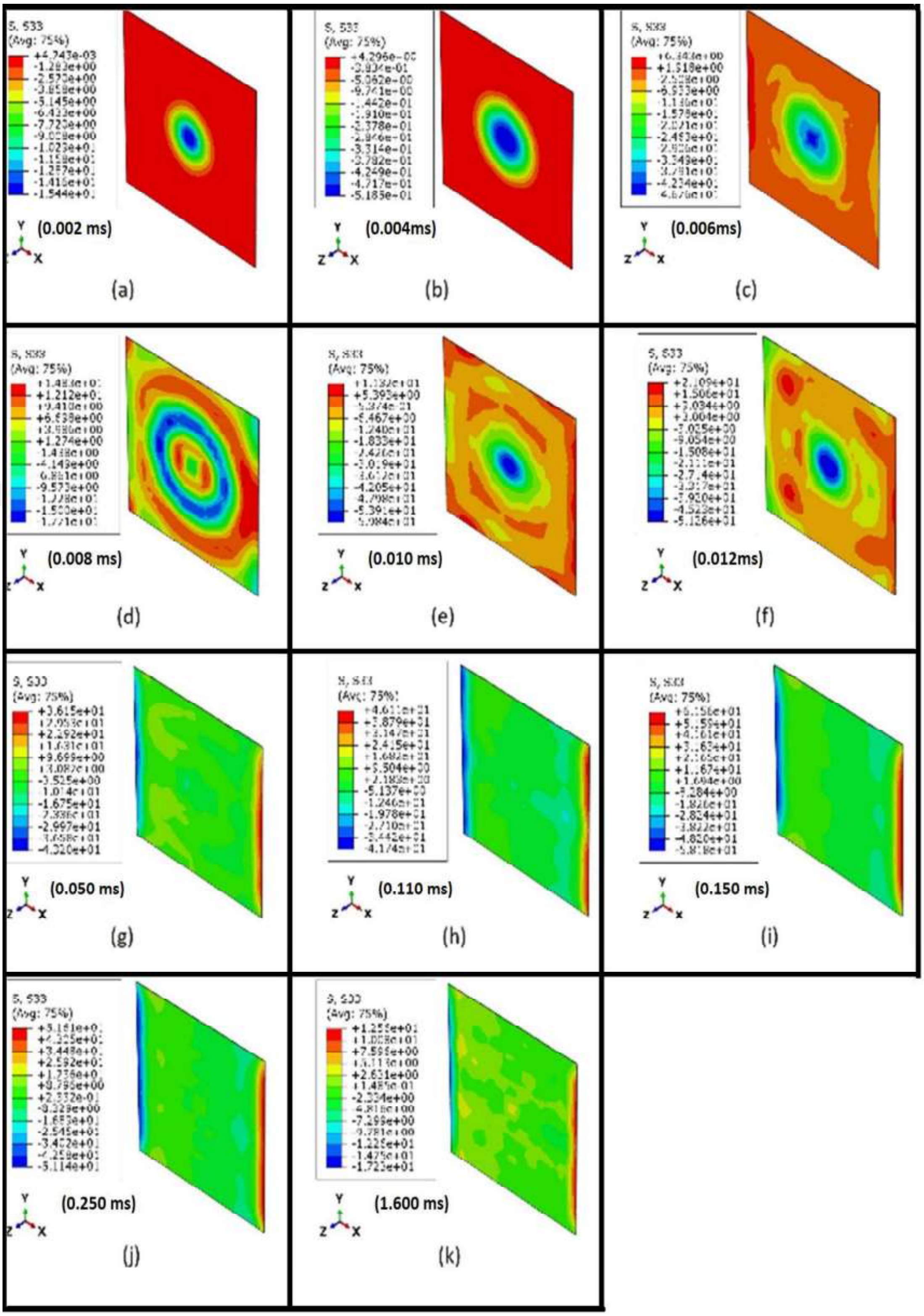

Figure 5.9. The predicted time-dependent normal stress (S33) of the adhesive layer under the impacted loading

Stress maps of the impacted adhesive layer are shown in Figure 5.9 that presents normal compression and tensile stresses (S33) in the z direction. The figure shows that at the very beginning of the impact the adhesive layer is in compression in the middle part, but mainly in tension beyond this part, presented in blue and red colors, respectively. This is especially clear for the a and b regions presented in Figure 5.9, in which the compression stresses are dominant, about 15 MPa and 52 MPa, but the tensile stresses are ignorable, about 0.005 MPa and 4 MPa, respectively. While the S33 stresses in compressions are still effective in the remaining regions, c-k, and has a maximum value of about 60 MPa in region e, those in tensions start increasing in region c, and has a maximum value of about 62 MPa in region i. It should be noted that as the effect of the impact comes to an end, the joint under the inertia force keeps to bending in the z direction. This bending behavior causes the stresses to decay in the middle part of the layer but concentrate at the edges, at the ends of the overlap. This can be seen clearly in Figure 4.10 that indicates the von Mises stresses (S) in the layer. It seems the values of the stress fluctuate in the different parts of the regions, a-k, and it reaches a maximum value of about 47 MPa at the edges (see Figure 5.10i) for a short time and then decreases.

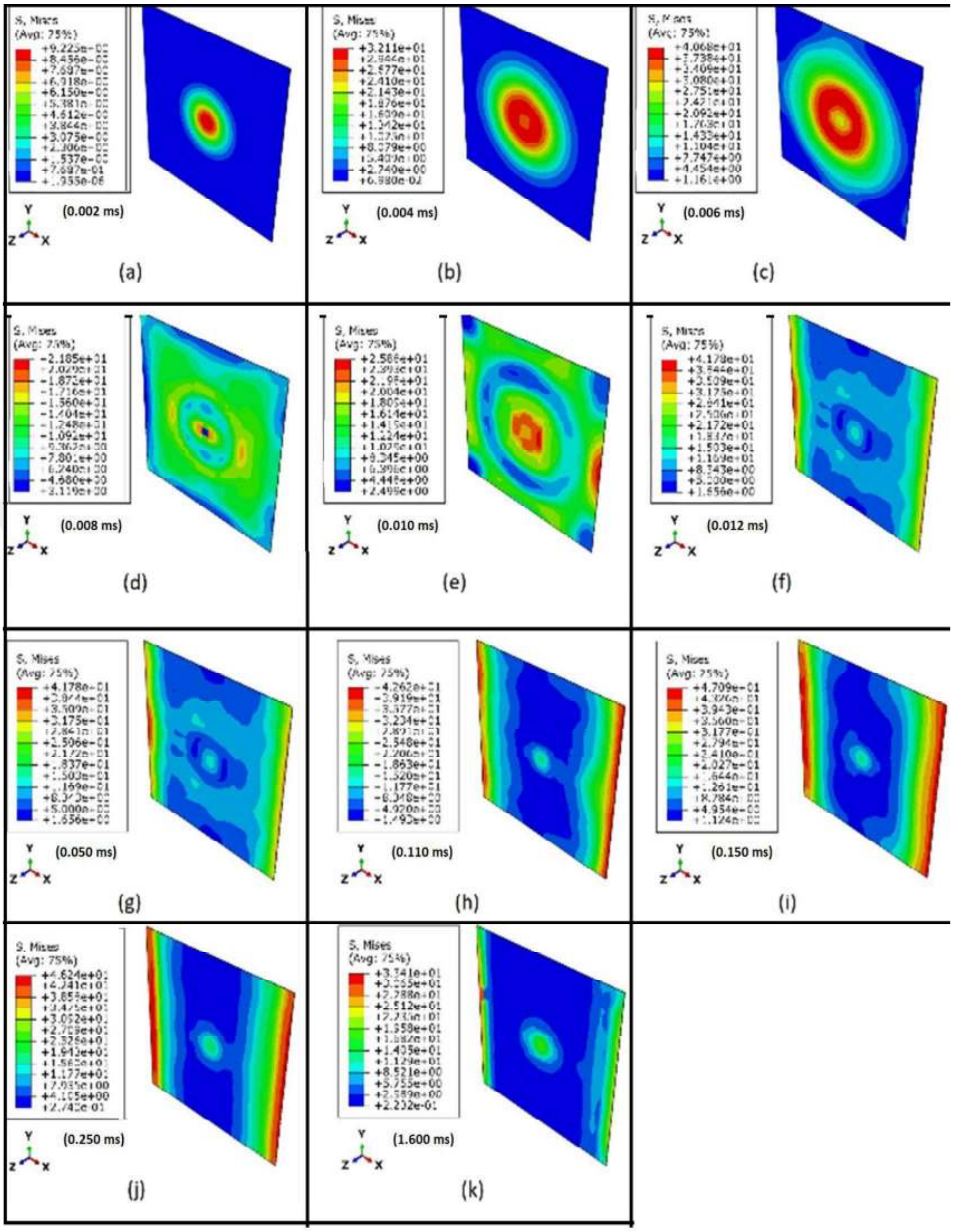

Figure 5.10. The predicted time-dependent von Mises stress (S) of the adhesive layer under the impacted loading

It is believed that the stress concentrations at the edges occurs due to the excessive displacement of the joint that experiences free vibrations after the impact. Figure 5.9i shows that while one edge in compression, the other is in tensile (peeling) stress that is considered as one of the most effective cause of the joint failure in the adhesive layer. However, if Figure 5.10i is examined closely, the peeling stress is limited in the very small part of the bonded region where excessive adhesive (spew fillet) exists that normally decreases the peeling effects and delays the failure [46]. As a matter of course, any failure of the adhesive layer is not expected due to the impact taking place. It should be noted that the spew fillet did not include in the numerical modal. It is also worth pointing out that the input data used in the modal were measured under the quasi-static conditions, however, real behavior of the adhesive layer under the impact conditions is expected to be strain-rate dependent [47] that implies the maximum stress increases while the strain to failure decreases in terms of the stress-strain curve subjected to high-speed tests. For the current study, the failure prediction of the adhesive layer was made according to quasi-static stress-strain curves shown in Figure, the worst-case scenario for the failure predictions.

Figure 5.11 indicates a predicted three-dimensional (3-D) shape of the projectile at the time when the impact takes place and comes to an end. It is seen that the projectile experiences a full plastic deformation.

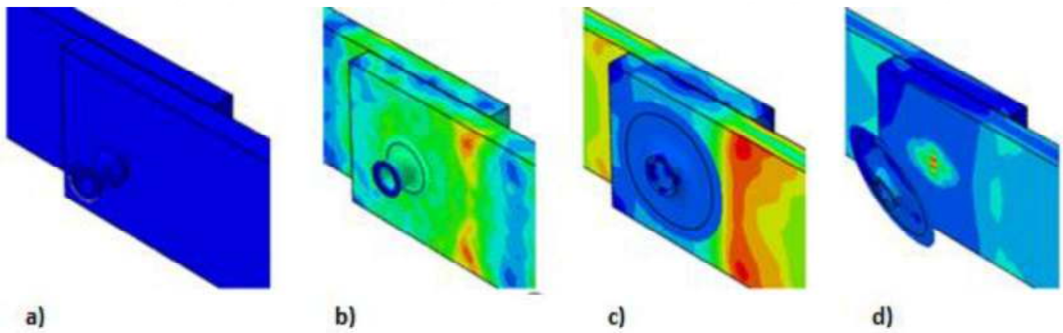

Figure 5.11. The predicted 3-D mechanical behavior of the projectile during the impact process

Figure 5.12 shows representative force-displacement curves obtained from the quasi-static tensile test after impact using the 100 kN Besmak Universal Testing Machine. Two different SLJs were subjected to the test; while one was a non-impacted specimen, the other was an impacted one. It seen that the specimen subjected to the impact loading has the same amount of failure load as the non-impacted one does. This clearly shows that the experimental results validate the numerical ones.

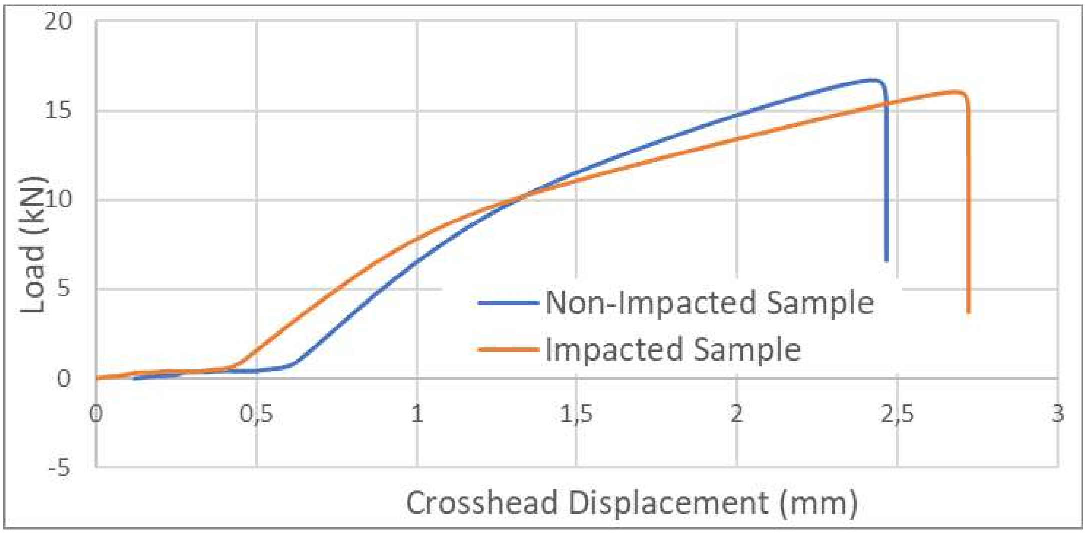

Figure 5.12 Force-displacement curves obtained from the quasi-static tensile test.

Although the numerical test results provide important information in the worst-case scenario, a new numerical analysis was run using the Johnson-cook material model, which is known to be more suitable for high-speed strain behavior in the metals.

5.2 To Prediction Metal to Metal Bonded Joints With Johnson-Cook Material Model.

5.2.1 Johnson-Cook Material Model Parameters

For the prediction behavior of the SLJ, the projectile and the adherends were treated as the materials obeying the Johnson-Cook model [48] that takes into consideration the effects of strain rate, strain hardening and temperature of the materials under different strain rate loadings. The Johnson-Cook material model parameters used for the analysis is tabulated in Table 5.1.

Table 5.1. Johnson-Cook parameters used in the numerila analysis for lead projectile and aluminium adherends.

Materials	*A* (MPa)	*B* (MPa)	*n*(-)	*m*(-)	T_r (K)	T_m (K)	*Co(-)*	ε_0*(-)*
Lead	24	300	1.00	1.00	298	925	0.1	0.0005
Aluminium	324	114	0.42	0.34	293	893	0.002	1

A, B, n, m, Co and ε0 are the material constants which can be determined from tensile and compression tests conducted at different strain rates and temperatures. Tm and Tr stand for melting temperature and room temperature, respectively [48,51].

5.2.2 Numerical Works

The maximum stress behavior of the adhesive at the impacting velocity (288 m/s) was assumed to be five times higher than that under quasi-static, proposed by a previous investigation [49]. Figure 5.13 shows the tensile stress-strain curve of the adhesive obtained from the quasi-static test, and also an elastic-perfectly plastic behavior used in the analysis. It is worth noting that the maximum stress of the adhesive is about 47.8 MPa obtained experimentally from the quasi-static, which was multiplied by 5 to obtain the maximum stress value (239 MPa) as input data for the current analysis. The elastic modulus as input data is the same as quasi-static value, 2.3 GPa (Table 4.1).

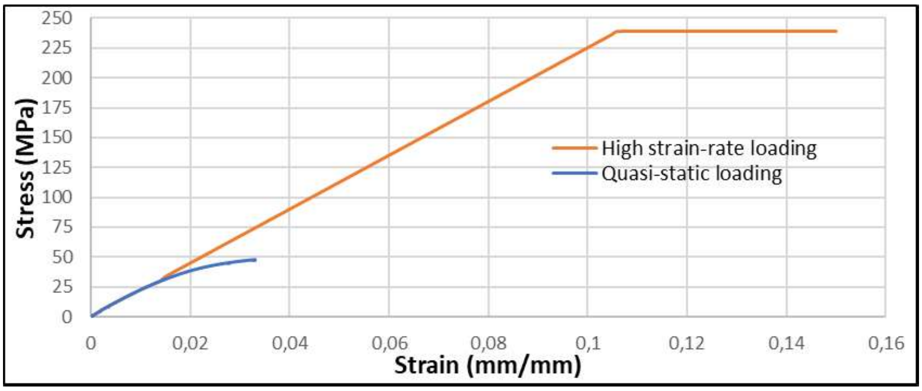

Figure 5.13 Tensile stress-strain curve of the adhesive layer used in the J-C numerical analysis.

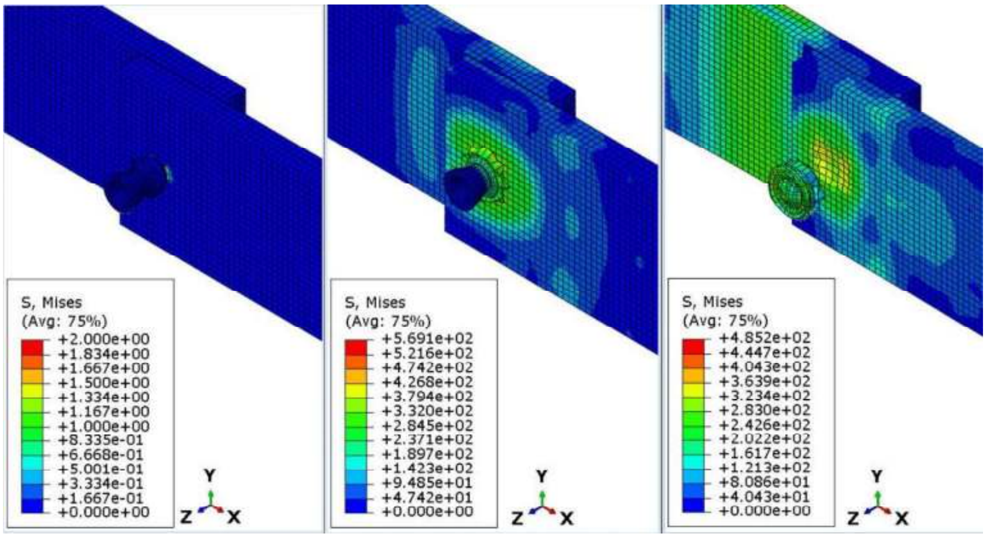

Figure 5.14 A three-dimensional numerical prediction of the von Mises stresses of the joints under impact of the projectile with 288 m/s.

Prediction of the von Mises stresses is presented in the figure 5.14 for three different periods of the impacting time; a) initial contact, b) full contact, and c) rebounding of the projectile. It is seen that a maximum stress is predicted when a full contact of the projectile and the adherend takes places (see Figure 5.15b), and then the stress tends to decrease when the projectile rebounds (see Figure 5.15c). Namely, the stress has a maximum value of about 569 MPa and then diminishes a value of about 485 MPa, considered quite high compared to the initial contact shown in Figure 5.15a, about 2 MPa.

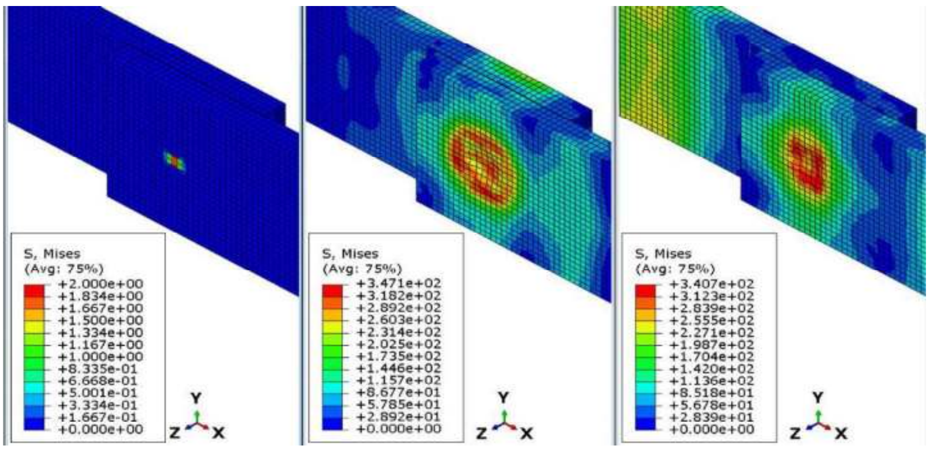

Figure 5.15 A three-dimensional numerical prediction of the von Mises stresses of the adherends under impact of the projectile with 288 m/s.

It is also worth pointing out that the final predicted shape of the projectile shown in Figure 5.15c is validated experimentally as shown in Figure 5.16 b.

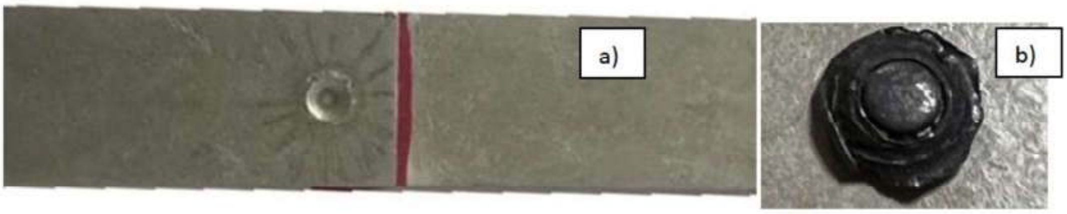

Figure 5.16. Real image of the hallow on the adherend (a) and of the projectile (b) after the ballistic test.

Von-Mises stress maps for the adhesive layer of the joint with 15 mm overlap length are indicated in Figure 5.17 that tells a partial failure is possible when the projectile has a complete contact with the specimen (see Figure 5.17a). This is mainly because the maximum value of the uniaxial stress, 239 MPa, shown in Figure 5.13, is nearly reached by the stress taking place in the impacted adhesive layer, about 238 MPa. It is seen from Figure 5.17a that the highest predicted stress levels occur not only in the middle but also at the left edge of the layer that is considered as one of the critical region for adhesive layer to fail, for a configuration of the adhesively bonded SLJ [49,50]. On the other hand, the stress value seems to diminish in Figure 5.17b, about 125 MPa. This can mainly be attributed to the joint behavior after the projectile rebounds. It is worth pointing out that spew fillets at both edges of the overlap ends have also been included in the analysis, which is formed due to the excessive adhesive during manufacturing processes.

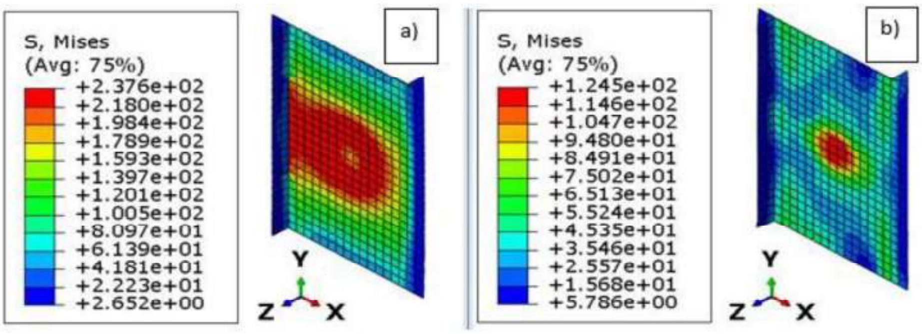

Figure 5.17 A three-dimensional numerical prediction of the von Mises stresses of the adhesive layer with 15 mm overlap length under impact of the projectile with 288 m/s.

Figure 5.18 shows the stress maps of the joint with 25 mm overlap length, which has different stress distributions from Figure 5.18; a maximum stress of about 222 MPa is predicted for this overlap length and this stress is mainly concentrated just in the middle of the layer (see Figure 5.18b). Nevertheless, stress distributions near the edges of the overlap is relatively small, about 90 MPa or even less (see Figure 5.17a), which implies no failure in the joint. Figure 5.17b indicates the stress distribution in the layer after the projectile rebounds, a decrement in the value, a maximum value of about 132 MPa.

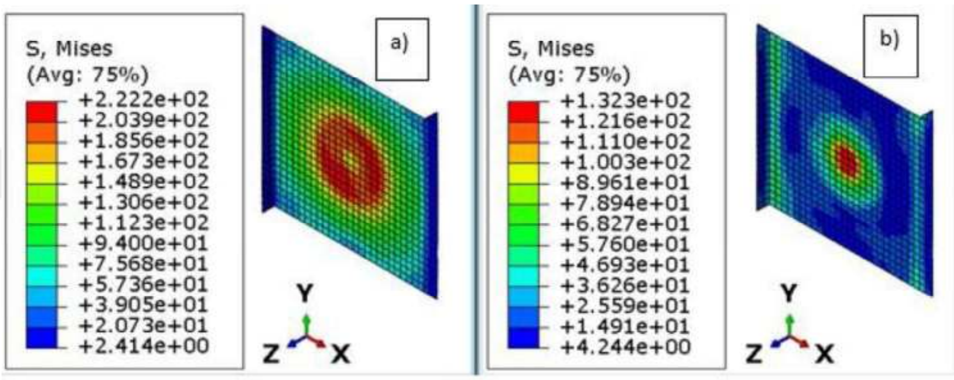

Figure 5.18 A three-dimensional numerical prediction of the von Mises stresses of the adhesive layer with 25 mm overlap length under impact of the projectile with 288 m/s.

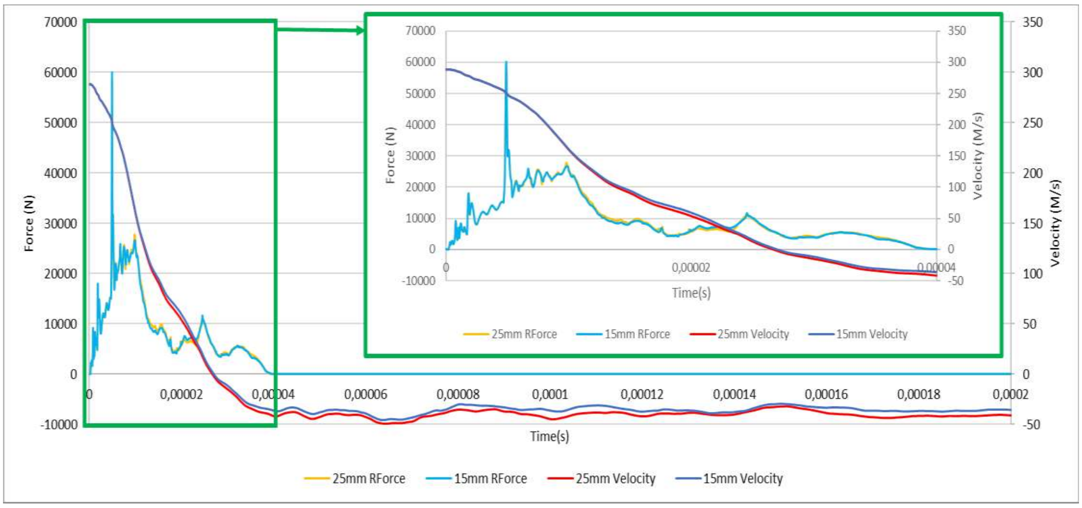

Figure 5.19 A numerical curve of johnson-cook dynamic load and velocity versus time from the impacted joints with the 15 mm and 25 mm overlap lengths.

Figure 5.19 illustrates the total force-time and average velocity-time curves of the projectile for the numerical models prepared with the johnson-cook material model with 15 and 25 mm overlap length. Note that the maximum force exerted by the lead before (fig 5.7) is almost close in the new model (Fig 5.19) as well, given the quasi-static model. However, it is seen that the contact time between the lead and the sample has decreased from 0.16 ms to 0.04 ms. In the johnson-cook model, it is also seen that the average velocity of the bullet is negative after 0.027 ms. The reason for the shortening of the contact time of the bullet is thought to be a more rigid behavior of the material depending on the deformation rate because of using the johnson-cook material model. Numerical solution could not be obtained with the test results obtained in quasi static conditions at speeds above 100m/s for high strain condition. Consistency could not be observed as quite high deformations occurred. In the Johnson Cook material model, on the other hand, at 288 m/s velocities, it is obvious that quite consistent and acceptable results are obtained when the test results are examined. The dynamic numerical analysis that run with the data obtained by quasi-static tests, was not yield satisfactory for the cases with high deformation rates. Because the materials under the dynamic investigation are have time dependent strain rates.

5.2.3 Experimental Works

To get a clear idea about possible effects of the projectile with 288 m/s velocity on the adhesive joints, the same impacted specimens were also subjected to quasi-static tensile tests using a Besmak BMT-S 100 kN universal testing machine.

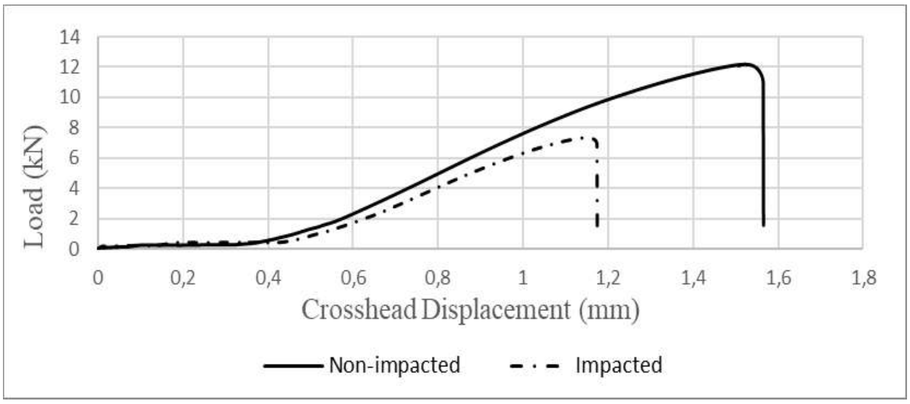

Figure 5.20 A representative curve of quasi-static load verses crosshead displacements from the non-impacted and impacted joints with the 15 mm overlap length.

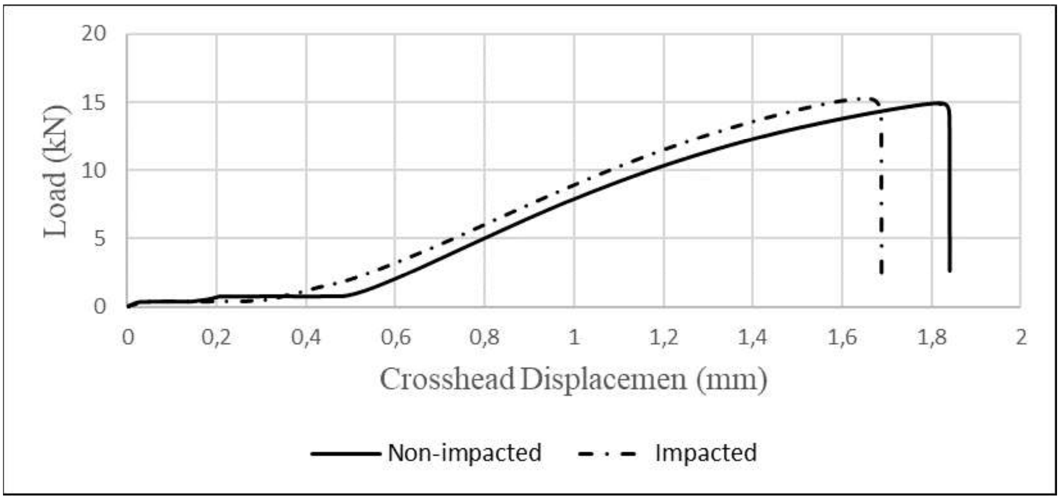

Figure 5.21 A representative curve of quasi-static load verses crosshead displacements from the non-impacted and impacted joints with the 25 mm overlap length.

The impacted joints were compared to non-imapcted ones. Figure 5.20 and Figure 5.21 show quasi-static test performance of the joints after impact with 15 mm and 25 mm overlap lengths, respectively. It is seen that while a decrement in the former is the case, there is no clear difference in the performance of the non-impacted and impacted specimens of the latter.

The joints with 15 mm overlap length seem to be affected by the projectile and have some permenant damage that leads to a decrement of about 40 % in the load to failure; while the load of the non-impacted specimens is about 12.16 kN, that of the impacted one is about 7.32 kN. Contrary to these joints, those with 25 mm overlap length have about 15 kN of the load to failure, for the both types, impacted and non-impacted. These experimental results are supported by the numerical ones presented in Figure 5.17 and Figure 5.18, which predicts possible failure in the adhesive layer.

CONCLUSION

In this thesis, the performance of adhesively-bonded joints of laminated glass-fiber (GF) and carbon fiber (CF)-reinforced polymer matrix composite materials were investigated under tensile and bending loadings. In general, a good agreement between the experimental and numerical results were obtained. For the tensile and bending loading conditions, the joints with the glass fiber adherends of 10°, 20°, 45°, 55° fiber orientations and with 15, 25 and 40mm overlap lengths were investigated. The same conducted for the joints with carbon fiber adherends with 15, 25, 40 mm overlap lengths and 2 and 3mm thicknesses. For the GF orientation case, the maximum load obtained from different loading modes increased when the ply angle decreased, and more uniform distribution of σ11 was observed on the adherend excluding its both ends when the overlap length was increased. In the case of the CF adherends with different thicknesses, there were mainly two different failure mechanisms for the tensile loading case; a failure in the adhesive layer resulting in cohesive failure, and mixed failure, partly the adhesive layer and also the composite layers for those with 40 mm overlap length. For the bending loading case, all the failure occurred in the plies bonded to the adhesive layer.

In the dynamic (vibration) tests; effects of the straps on the dynamic performance of the Single Strap Joints (SSJs) were studied. It seemed the straps with ±450 angle plies in the different stacking sequences were able to enhance the damping performance of the joints, compared to those with the unidirectional (00 angle) ones. Contribution of the longer straps (45 mm) to the damping performance of the joints was negligible, although a small decrease was observed in the value of the flexural rigidity, compared to the those with the shorter straps (25 mm).

Finally, metal to metal (aluminum) single lap joint configurations in clamped-clamped boundary conditions were tested and modeled under high loading rate. A three-dimensional model was created using a Finite Element Model via ABAQUS package program. The predicted impacted behavior of the joint was presented for the bullet with 1.25 gr weight and 100 m/s velocity. The velocity of the bullet impacting the joint and the dynamic load against time the joint experiences were predicted successfully.

The predicted value was validated using an experimental set-up that enabled the joint to be impacted under similar conditions to the model did. After the impact, the stress concentrations at the edges occurs due to the excessive displacement of the joint that experiences free vibrations. Although the numerical test results provided important information in the worst-case scenario, a new numerical analysis was undertaken using the Johnson-cook material model, which is known to be more suitable for the ballistic case. It was obtained that the experimental and numerical results were in agreement; when the impacted joints were compared to the non-impacted ones under the static conditions, it was found that the impacted ones with the 15 mm overlap length decreased about 40 % in the load to failure compared to non-impacted ones. Unlike these joints, those with the 25 mm overlap length did not seem to be affected by the projectile. Finally, dynamically deforming materials behave differently from their quasi-static properties because they have time-dependent strain rates.

REFERENCES

[1] Kashtalyan, Maria., "*Composite Materials for Aircraft Structures*" 2nd Edition Edited by A. A. Baker and M. L. Scott American Institute of Aeronautics and Astronautics, The Aeronautical Journal., 122, 842-843., 2004.

[2] Adams RD, Comyn J and Wake WC. Structural Adhesive Joints in Engineering, 2nd Edition. Elsevier Applied Science, 1997.

[3] Budhe S, Banea MD de Barros S and da Silva LFM., "*An updated review of adhesively bonded joints in composite materials",* International Journal of Adhesion & Adhesives, 72: 30-42., 2017

[4] Mohan J, Ivanković A and Murphy N. "*Mode I fracture toughness of co-cured and secondary bondedcomposite joints."* International Journal of Adhesion and Adhesives, 51: 13-22, 2014.

[5] Mohan J, Ivanković A and Murphy N., *"Mixed-mode fracture toughness of co-cured and secondary bonded composite joints."* Engineering Fracture Mechanics, 134: 148-167,2015.

[6] Ji G, Ouyang Z, Li G, Ibekwe S and Pang SS., *"Effects of adhesive thickness on global and local Mode-I interfacial fracture of bonded joints. International Journal of Solids and Structures*", 47: 2445-2458, 2010.

[7] Xu W and Wei Y. "*Strength and interface failure mechanism of adhesive joints."* International Journal of Adhesion and Adhesives, 34: 80-92, 2012.

[8] 18 Mahi BE, Benrahou KH, Belakhdar K, Tounsi A and Bedia EAA. "*Effect of the tapered end of a FRP plate on the interfacial stresses in a strengthened beam used in civil engineering applications."* Mechanics of Composite Materials, 50: 467-476, 2014.

[9] Li J, Yan Y, Zhang T and Liang Z. "*Experimental study of adhesively bonded CFRP joints subjected to tensile loads.*" International Journal of Adhesion and Adhesives, 57: 95-104, 2015.

[10] Campilho RDSG, de Mouro MFSF and Domingues JJMS. *"Numerical prediction on the tensile residual strength of repaired CFRP under different geometric changes."* International Journal of Adhesion and Adhesives, 29: 195-205, 2009.

[11] Marques EAS, Campilho RDSG and da Silva LFM. *"Geometrical study of mixed adhesive joints for high temperature applications.",* Journal of Adhesion Science and Technology 30: 691-707, 2016.

[12] Marques EAS, Campilho RDSG and da Silva LFM. *"Geometrical study of mixed adhesive joints for high temperature applications."* Journal of Adhesion Science and Technology, 30: 691-707, 2016.

[13] Kadioglu F, Demiral M, Avil E, Ercan ME and Aydogan T. "*Performance of Adhesively-bonded Joints of Laminated Composite Materials under Different Loading Modes.*", AIAA/ASCE/AHS/ASC Structures, Structural Dynamics, and Materials Conference, AIAA SciTech Forum (AIAA 2018-0222), 2018.

[14] Meneghetti G, Quaresimin M and Ricotta M. "*Influence of the interface ply orientation on the fatigue behaviour of bonded joints in composite materials.*" International Journal of Fatigue, 32: 82-93, 2010.

[15] Kadioglu F and Puskul H. "*Effects of Different Fiber Orientations on the Shear Strength Performance of Composite Adhesive Joints. World Academy of Science"*, Engineering and Technology International Journal of Materials and Metallurgical Engineering, 10: 65-68, 2016.

[16] Araújo, H.A.M., Machado, J.J.M., Marques, E.A.S., and Da Silva, L.F.M., *"Dynamic Behavior of Composite Adhesive Joints for the Automotive Industry",* Composite Structures, Vol: 171, 1, pp. 549–561, 2017.

[17] Takeda, T., and Narita, F., *"Fracture Behavior and Crack Sensing Capability of Bonded Carbon Fiber Composite Joints with Carbon Nanotube-Based Polymer Adhesive Layer under Mode I Loading"*, Composites Science and Technology, Vol: 146, pp. 26–33, 2017.

[18] Lapczyk, I., and Hurtado, J.A., *"Progressive damage modeling in fiber-reinforced materials"*, Composites Part A: Applied Science and Manufacturing, Vol: 38(11), pp.2333-2341, 2007.

[19] Yokoyama T. *"Experimental determination of impact tensile properties of adhesive butt joints with the split Hopkinson bar.*" The Journal of Strain Analysis for Engineering Design.,38(3):233-245, 2003.

[20] Rashed A, Yazdani M, Babaluo A, Hajizadeh Parvin P. "*Investigation on high-velocity impact performance of multi-layered alumina ceramic armors with polymeric interlayers."* Journal of Composite Materials., 50(25):3561-3576, 2016.

[21] Kelly, G., *"Load transfer in hybrid (bonded/bolted) composite single-lap joints."* Composite Structures, 69, 35-43, 2004.

[22] Bois, C., Wargnier, H., Wahl, J. C. ve Goff, E.L. *"An analytical model for the strength prediction of hybrid (bolted/bonded) composite joints."* Composite Structures, 97, 252 – 260., 2013.

[23] Chan, W. S. ve Vedhagiri, S., *"Analysis of composite bonded / bolted joints used in repairing."* Journal of Composite Materials, 35, 1045-1061, 2001.

[24] Meyer CS, Haque BZ, O'Brien DJ, et al. *"Mesoscale ballistic damage mechanisms of a single-layer woven glass/epoxy composite."* International Journal of Impact Engineering, 113: 118–131., 2018.

[25] Bonyi E, Meyer CS, Kioko B, et al. *"Assessment and quantification of ballistic impact damage of a single-layer woven fabric composite."* International Journal of Damage Mechanics., 28(2):249-269, 2019.

[26] A. Seyed Yaghoubi, B. Liaw. "*Effect of lay-up orientation on ballistic impact behaviors of GLARE 5 FML beams*", International Journal of Impact Engineering, 54: 138-148, 2013.

[27] Ercan Sevkat, Benjamin Liaw, Feridun Delale, Basavaraju B. Raju., *"A combined experimental and numerical approach to study ballistic impact response of S2-glass fiber/toughened epoxy composite beams*, Composites Science and Technology", Vol 69, Issues 7–8, Pages 965-982, 2009.

[28] T. J. Holmquist, G. R. Johnson, W. A. Gooch, "Modeling the 14.5 mm BS41 projectile for ballistic impact computations" Transactions on State of the Art in Science and Engineering, Vol 75, WIT Press, 2014.

[29] Aviral Shrot, Martin Bäker, *"Determination of Johnson–Cook parameters from machining simulations."*, Computational Materials Science, Volume 52, Issue 1, Pages 298-304, 2012.

[30] Nitin Thakur, Pramod Kumar, Rabinder Singh Bharj, *"Effect of Variation of Johnson-Cook Parameters on Kinetic Energy and Simulation of 4340 Steel Projectile,"* Materials Today: Proceedings, Volume 5, Issue 14, Part 2, Pages 27884-27892, 2018.

[31] Xuemei Wang, Jun Shi, "*Validation of Johnson-Cook plasticity and damage model using impact experiment*", International Journal of Impact Engineering, Volume 60, Pages 67-75, 2013.

[32] Shokrieh, Mahmood M et al. *"A dynamic constitutive-micromechanical model to predict the strain rate-dependent mechanical behavior of carbon nanofiber/epoxy nanocomposites."* Iranian Polymer Journal 25: 487-501, 2016.

[33] Ding-Ni Zhang, Qian-Qian Shangguan, Can-Jun Xie, Fu Liu, *"A modified Johnson–Cook model of dynamic tensile behaviors for 7075-T6 Aluminum alloy"*, Journal of Alloys and Compounds, Volume 619, Pages 186-194, 2015.

[34] Gollins, Kenneth & Elvin, Niell & Delale, Feridun. *"Characterization of Adhesive Joints Under High-Speed Normal Impact: Part II – Numerical Studies."* International Journal of Adhesion and Adhesives. 98. 102530, 2020.

[35] Tamrakar S, Ganesh R, Sockalingam S, Haque BZ (Gama), Gillespie JW. *"Strain rate-dependent large deformation inelastic behavior of an epoxy resin.",* Journal of Composite Materials., 54(1):71-87, 2020.

[36] ABAQUS,V.6.14 Documentation, "Dassault Systemes Simulia Corporation", 2014.

[37] Kaw, Authar K., "*Mechanics of composite materials*." Boca Raton: Taylor & Francis Group., 2006.

[38] Mallick, P.K. "*Fibre Reinforced Composites: Materials, Manufacturing and Design."* 2nd Edition, Marcel Dekker Inc., New York., 1993.

[39] Besergil, B. *"Kompozitler"*, Ankara; Gazi Kitabevi., 2016.

[40] Kaman, M. O., *"Effect of fiber orientation on fracture toughness of laminated composite plates [0/θ] s."* Engineering Fracture Mechanics, *78*(13), 2521-2534, (2011).

[41] Standard Test Method for Apparent Shear Strength of Single-Lap-Joint Adhesively Bonded Metal Specimens by Tension Loading (Metal-to-Metal): ASTM-D1002-10.

[42] Kadioglu, F., Avil, E., Ercan, M. E., & Aydogan, T., *"Effects of different overlap lengths and composite adherend thicknesses on the performance of adhesively-bonded joints under tensile and bending loadings.*" In IOP Conference Series: Materials Science and Engineering (Vol. 369, No. 1, p. 012034). IOP Publishing., 2018.

[43] Unver, E., Kadioglu, F., Ercan, M. E. (2021) *"The Straps with Different Fiber Orientations Affecting the Dynamic Behavior of the Single Strap Joints."*, SAMPE neXus 2021, https://www.nasampe.org/store/viewproduct.aspx?id=18598533 [Date: June 29, 2021].

[44] Hexel Corporation, "*Data Sheets / Prepreg* [online]" https://www.hexcel.com/Resources/DataSheets/Prepreg [Date: 01.02.2022]

[45] 3M Corporation, "*3M Structural Adhesive Films* [Online]" https://www.3m.com/3M/en_US/p/c/adhesives/structural/films/ [Date:01.02.*2022]*

[46] Adams R.D, Peppiatt N.A., "*Stress analysis of adhesive-bonded lap joints.",* Journal of Strain Analysis for Engineering. 9, 185-196., 1974.

[47] Kadioglu, F. and Adams R. D., "*Flexible adhesives for automotive application under impact loading,"* International Journal of Adhesion & Adhesives 56, 73–78., 2015.

[48] Goglio L, L. Peroni M. Peroni, and M. Rossetto., *"High Strain-Rate Compression and Tension Behaviour of An Epoxy Bi-Component Adhesive,"* Int J Adhes Adhes., 28(7):329–39., 2008.

[49] Johnson, G.R. and W.H. Cook. "*A Constitutive Model and Data for Metal Subjected to Large Strains, High Strain Rates and High Temperature*," Proceedings of the 7th International Symposium on Ballistics. The Hague, Netherlands. 1983.

[50] Adams, R.D. and N.A. Peppiatt., "*Effect of Poisson's Ratio Strains in Adherends on Stresses of an Idealized Lap Joint*," J. Strain Anal. Eng., 8(2):134-139., 1974.

[51] Walker, J.D., *"Modern Impact and Penetration Mechanics"*, Cambridge University Press., Cambridge/UK, 2021

[52] Stronge, W., *"Impact Mechanics"* 2nd Edition., Cambridge University Press., Cambridge/UK, 2018.

[53] C. Lakshmana Rao, V. Narayanamurthy, K. R. Y. Simha, *"Applied Impact Mechanics"* 1st Edition., John Wiley & Sons Ltd., Chichester/ West Sussex/ UK., 2016.

[54] Xu, Lizhi, Chun Cheng, Chengxin Du, Zhaoxiu Jiang, Zhonghua Du, and Guangfa Gao. "*Semi-Crystalline Polymers Applied to Taylor Impact Test: Constitutive, Experimental and FEM Analysis*" *Polymers* 12, no. 7: 1615., 2020.

[55] Gray, G. T. (Rusty), Maudlin, P. J., Hull, L. M., Zuo, Q. K., & Chen, S.-R., *"Predicting material strength, damage, and fracture The synergy between experiment and modeling. Journal of Failure Analysis and Prevention"*, Journal of Failure Analysis and Prevention, 5(3) : 7–17, 2005.

[56] Ercan, M.E., Kadioglu, F. *"Mechanical behavior of adhesively-bonded joints under high loading rates"*, 36th Technical Conference of the American Society for Composites, Conference of Composites Ingenuity Taking on Challenges in Environment-Energy-Economy, 1230–1241, 2021.

[57] U.S. Department of Energy, Material Science., *"Fundamentals Handbook",* Volume 1 and 2." Washington, D.C., 1993.

[58] Den Hartog JP, "*Mechanical Vibrations*", McGraw-Hill Book Company Inc, New York, London, 1947.